

# The Indoor-Training Effect: unexpected gains from distribution shifts in the transition function

Serena Bono<sup>1</sup>, Spandan Madan<sup>2</sup>, Ishaan Grover<sup>1</sup> Mao Yasueda<sup>3</sup>,  
Cynthia Breazeal<sup>1</sup>, Hanspeter Pfister<sup>2</sup>, Gabriel Kreiman<sup>2</sup>

<sup>1</sup>MIT Media Lab <sup>2</sup>Harvard University <sup>3</sup>Yale University

## Abstract

Is it better to perform tennis training in a pristine indoor environment or a noisy outdoor one? To model this problem, here we investigate whether shifts in the transition probabilities between the training and testing environments in reinforcement learning problems can lead to better performance under certain conditions. We generate new Markov Decision Processes (MDPs) starting from a given MDP, by adding quantifiable, parametric noise into the transition function. We refer to this process as *Noise Injection* and the resulting environments as  $\delta$ -environments. This process allows us to create variations of the same environment with quantitative control over noise serving as a metric of distance between environments. Conventional wisdom suggests that training and testing on the same MDP should yield the best results. In stark contrast, we observe that agents can perform better when trained on the noise-free environment and tested on the noisy  $\delta$ -environments, compared to training and testing on the same  $\delta$ -environments. We confirm that this finding extends beyond noise variations: it is possible to showcase the same phenomenon in ATARI game variations including varying Ghost behaviour in PacMan, and Paddle behaviour in Pong. We demonstrate this intriguing behaviour across 60 different variations of ATARI games, including PacMan, Pong, and Breakout. We refer to this phenomenon as the *Indoor-Training Effect*. Code to reproduce our experiments and to implement *Noise Injection* can be found at <https://bit.ly/3X6CTYk>.

## Introduction

Consider the process of learning how to play tennis. You might think that the best way to prepare for an outdoor match is to train under the same outdoor conditions you will face during the match. However, training in a calm, noise-free indoor environment instead can help focus on mastering the fundamentals of tennis without the added challenge of sources of noise like wind. We refer to this phenomenon as the *Indoor-Training Effect*. Here we model this problem using reinforcement learning (RL) agents. Surprisingly, we found that under certain conditions, training in a noise-free environment can lead to better performance when tested in a noisy environment—just like tennis. This phenomenon challenges our intuitions about the standard way to train RL

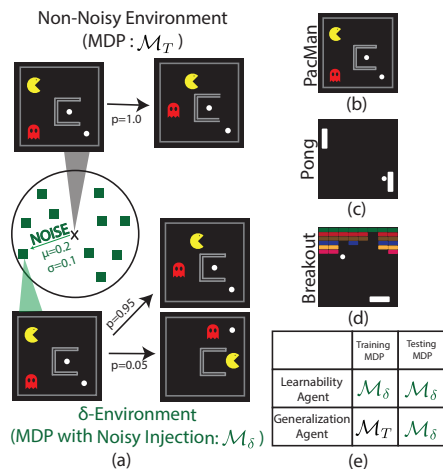


Figure 1: *ATARI* games modified with *Noise Injection*. (a) In the original Target Environment ( $\mathcal{M}_T$ ), when the agent (PacMan) moves right, PacMan moves right with probability 1.0. Noise Injection allows us to create multiple worlds in the vicinity of this environment by adding controlled Gaussian noise ( $\delta$ ) to the original Transition Function ( $T$ ). When the agent takes the action *right* in these  $\delta$ -environments, with a low probability the game may transition to a state which would not be possible in non-noisy PacMan. For brevity, we refer to these transitions as non-standard transitions which are 0 probability in the original Target, but are now possible. Experiments with noise injection are presented on three ATARI games—(b) PacMan, (c) Pong, and (d) Breakout. (e) We compare two agents with these environments—a Learnability agent trained and tested on the same target environment ( $\mathcal{M}_\delta$ ), and a Generalization agent trained on a different MDP ( $\mathcal{M}_T$ ) and tested on  $\mathcal{M}_\delta$ .

agents where conventional wisdom would suggest that the best approach to perform well on a target problem is to train an RL agent on the same test environment.

Environments in RL are usually described using Markov Decision Process (MDP). An MDP is defined by a State Space  $\mathcal{S}$ , an Action Space  $\mathcal{A}$ , a Transition Function  $\mathcal{T}$ , and a Reward Function  $\mathcal{R}$ . In practice, these parameters are assumed to be known or approximated with reasonable preci-

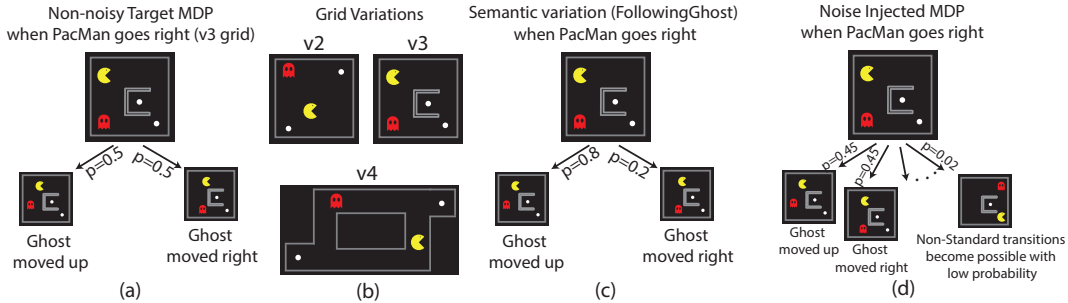


Figure 2: *Schematic illustration of variations for Pacman.* (a) Game dynamics when the agent picks the action *right* in a standard, non-noisy MDP for the v3 grid. The ghosts’ actions follow a uniform probability distribution over possible moves and move *up* or *right* with an equal probability of 0.5. This is referred to as a RandomGhost. (b) Grid variations for Pacman—v2, v3, and v4. These grids vary in size, positions of walls, and positions of food pellets. v2, v3, and v4 are designed to be increasingly harder. (c) Semantic variations whereby there is a meaningful change in the distribution of game elements. Here, a FollowingGhost is depicted which has a higher probability of taking a move that brings it closer to the Pacman (0.8). (d) Noise injected MDP generated by adding Gaussian noise to the standard transition function. Alongside states reachable by the ghost taking a legal move, non-standard transitions now become possible which result in the game reaching states otherwise unreachable.

sion (Bauerle and Glauner 2022; Goyal and Grand-Clement 2023). A significant challenge in RL is generalizing to environments that differ from the training environment (Cobbe et al. 2019; Kang et al. 2019; Devin et al. 2018). To address this, the RL community has focused on training agents capable of learning policies that perform well in novel, unseen environments at deployment time (Kirk et al. 2021; Moos et al. 2022a; OpenAI et al. 2019; Filos et al. 2020; Biedenkapp et al. 2020). The complexity of this task has called for ingenious ways of aligning the policy learned by the agent in training environments with the testing optimal policy. Notable approaches include using human feedback (Rummery and Niranjan 1994), using language (Tellex et al. 2011; Walter et al. 2013; Squire et al. 2015), and using vision (Guss et al. 2019; Osinski et al. 2020; Gopalan et al. 2017).

To study this, we explored zero-shot policy transfer where a policy trained in one environment is tested on a different environment. We extended past works which focused on uncertainty in the transition probabilities (Nilim and El Ghaoui 2005; Moos et al. 2022b; Goyal and Grand-Clement 2023), and propose a novel framework for studying zero-shot policy transfer in environments with controlled, quantifiable distribution shifts in the transition probabilities.

Our framework introduces these shifts by computing the transition function of an MDP, and adding small Gaussian noise to its entries. Starting with an environment ( $\mathcal{M}_T$ ), noise is sampled and added to it to obtain a new MDP ( $\mathcal{M}_\delta$ ). We refer to this approach as *Noise Injection* and the resulting new MDPs as  $\delta$ -environments as in Fig. 1. Noise injection introduces several non-standard transitions, which had zero probability in the original MDP. Multiple such environments can be created by sampling noise and the noise serves as a metric of distance between environments. This approach allows us to create multiple worlds starting from the same MDP, with quantitative control over the variations in the transition probabilities. An increase in the standard deviation of the Gaussian noise results in increasingly perturbed MDPs. We

report experiments with Noise Injection on multiple domains across three ATARI games—PacMan, Pong, and Breakout.

To study policy transfer we define two agents: a **Learnability Agent** ( $\mathcal{L}_\delta$ ) which is **trained and tested on the same  $\delta$ -environment** ( $\mathcal{M}_\delta$ ), and a **Generalization Agent** ( $\mathcal{G}_T$ ) which is **trained on the original noise-free environment** ( $\mathcal{M}_T$ ) **but tested on the  $\delta$ -environment** ( $\mathcal{M}_\delta$ ). Conventional wisdom suggests that the Learnability Agent should perform better as it is trained and tested on the same environment. However, our study across 60 MDPs built on ATARI games reveals a surprising finding—there are several cases where the Generalization Agent outperformed the Learnability Agent. We confirmed that this finding extends beyond our setup of noise injection and  $\delta$ -environments and also holds true for game variations including varying the Ghost behaviour in PacMan, and Paddle behaviour in Pong. We refer to these as semantic variations in MDPs.

In conclusion, to better understand this phenomenon we analyzed the exploration patterns of the Learnability and Generalization Agents, and the corresponding policies learned by them. Our analyses revealed that  $\mathcal{L}_\delta$  agents outperformed  $\mathcal{G}_T$  agents, as expected from the literature, when  $\mathcal{G}_T$  agents fail to explore the same State-Action pairs as the  $\mathcal{L}_\delta$  agents. In contrast, when there were no large differences in their exploration patterns, the performance of  $\mathcal{G}_T$  aligned or exceeded that of  $\mathcal{L}_\delta$  agent.

## Preliminaries: Reinforcement Learning

Similar to (Cederborg et al. 2015), our work considers Reinforcement Learning (RL) as a group of algorithms designed to solve problems formulated as Markov Decision Processes (MDPs). A Markov Decision Process is characterized by the tuple  $(\mathcal{S}, \mathcal{A}, \mathcal{T}, \mathcal{R}, \lambda)$ , representing the collection of potential world states ( $\mathcal{S}$ ), space of actions ( $\mathcal{A}$ ), the transition function ( $\mathcal{T} : \mathcal{S} \times \mathcal{A} \rightarrow \mathcal{P}(\mathcal{S})$ ), the reward function ( $\mathcal{R} : \mathcal{S} \times \mathcal{A} \rightarrow \mathcal{R}$ ), and a discount factor ( $0 < \gamma \leq 1$ ). The objective is to identify policies ( $\pi : \mathcal{S} \times \mathcal{A} \rightarrow \mathcal{R}$ ) that maximize cumulative

ATARI Game	Grid Variations	Noise Injected Variations	Semantic Variation	Total
PacMan	v2, v3, v4	$\delta = 0$ (No Noise) $\delta \sim \mathcal{N}(0, 0.1)$ $\delta \sim \mathcal{N}(0, 0.5)$	RandomGhost FollowingGhost ( $p = 0.3, 0.6$ ) TeleportingGhost ( $p = 0.5, 0.2$ )	33
Pong	p1, p2	$\delta = 0$ (No Noise) $\delta \sim \mathcal{N}(0, 0.1)$ $\delta \sim \mathcal{N}(0, 0.5)$	RandomPaddle FollowingPaddle ( $p = 0.3, 0.6$ )	18
Breakout	b1, b2, b3	$\delta = 0$ (No Noise) $\delta \sim \mathcal{N}(0, 0.1)$ $\delta \sim \mathcal{N}(0, 0.5)$	-	9

Table 1: **Overview of experimental protocol.** Our experiments include multiple variations of three ATARI games—PacMan, Pong, and Breakout. For each game, we have multiple grid variations. When introducing variations in these grids with noise injection, we report results for two levels of added noise—a low-noise setting:  $\delta \sim \mathcal{N}(0, 0.1)$ , and a high-noise setting:  $\delta \sim \mathcal{N}(0, 0.5)$ . Furthermore, for each grid we introduce further variations by modifying the distribution of the stochastic game element (ghost in PacMan, and the computer paddle in Pong). In all, we report results on 60 MDPs across these games.

rewards.

Q-learning (Watkins and Dayan 1992) and SARSA (Kaelbling, Littman, and Moore 1996) are two algorithms to learn such policies. Both Q-Learning and SARSA algorithms update the Q-values of state-action pairs, but they differ in their approaches. Q-Learning focuses on the maximum expected future rewards, and updates Q-values using the formula:

$$Q(s, a) \leftarrow Q(s, a) + \alpha \left[ r + \gamma \max_{a'} Q(s', a') - Q(s, a) \right] \quad (1)$$

where  $\alpha$  is the learning rate,  $\gamma$  is the discount factor, and  $s, s', a, a', r$  represent the current state, next state, current action, next action, and immediate reward, respectively.

On the other hand, SARSA updates Q-values based on the actual policy’s actions with the formula:

$$Q(s, a) \leftarrow Q(s, a) + \alpha [r + \gamma Q(s', a') - Q(s, a)] \quad (2)$$

Here the update incorporates both immediate rewards and the Q-value of the actual next action taken.

Agents need to balance two critical aspects: exploration and exploitation. Exploration involves trying potentially less optimal actions to understand the environment better. Conversely, exploitation means choosing actions known to yield high rewards. We report results with the Boltzmann and the  $\epsilon$ -greedy exploration strategies. Boltzmann exploration determines the probability of selecting an action as follows:

$$Pr_q(a) = \frac{e^{Q(s,a)/\tau}}{\sum_{a'} e^{Q(s,a')/\tau}} \quad (3)$$

The constant  $\tau$  is referred to as the temperature. On the other hand, the  $\epsilon$ -greedy strategy is simpler and more direct—the agent selects a random action with probability  $\epsilon$ , and the action with the highest Q-value with probability  $1 - \epsilon$ .

## Related Works

Generalization benchmarks in RL involve training and testing across different subsets of tasks, levels, or environments. Recent years have seen several generalization benchmarks, which include variations in the state space (Hafner 2021),

dynamics (Dulac-Arnold, Mankowitz, and Hester 2019), observation (Zhu et al. 2020), reward function (Bapst et al. 2019), and new game levels (Justesen et al. 2018), among others. There has also been recent work investigating generalization in Deep Reinforcement Learning (Zhu et al. 2023; Packer et al. 2018; Cobbe et al. 2019; Lyle et al. 2022). Combined, these tasks require explicit modeling of variations to effectively assess generalization, highlighting the need for robust evaluation protocols.

Contextual Markov Decision Processes (CMDP) provide a formal structure for this, where environments are sampled from a class of contexts, with agents trained on a subset and tested on a disjoint subset. These contexts are generated through two primary methods: Procedural Content Generation (PCG), which relies on a seed value for environment generation, and Controllable Environments (CE), which allow for manipulation of individual components. The integration of a suitable evaluation protocol with these contexts helps define the relationship between training and testing sets, which can range from interpolation to full extrapolation. Some examples of benchmarks using these frameworks include the OpenAI Procgen benchmark (Cobbe et al. 2020) and the Distracting Control Suite (Stone et al. 2021) for PCG (Ahmed et al. 2020) and RWRL (Dulac-Arnold, Mankowitz, and Hester 2019) for controllable environments. A major drawback in these benchmarks is the lack of a clearly defined metric for measuring how the distance between different contexts affects agent performance.

To solve this issue we draw inspiration from work studying generalization under controlled, quantifiable distribution shifts in computer vision. These studies include shifts in 3D rotation (Mondal, Dulberg, and Cohen 2022; Madan et al. 2023), category-viewpoint combinations (Madan et al. 2022a), incongruent scene context (Bomatter et al. 2021), novel light and viewpoint combinations (Sakai et al. 2022), object materials (Madan et al. 2022b) and textures (Geirhos et al. 2018; Michaelis et al. 2019), and non-canonical viewpoints (Barbu et al. 2019), among others.

## Generating MDPs for investigating generalization

We created 60 different MDPs across three ATARI games (PacMan, Pong, and Breakout) by varying grid layouts, distributions defining the stochasticity of different game elements, and modifying transition probabilities using Noise Injection (Fig. 2 and Table. 1). Here we outline these variations.

**Domains** We implemented all three ATARI games from scratch, building on the Berkeley PacMan Projects (DeNero, Klein, and Abbeel 2014). PacMan was modelled as an MDP characterized by the tuple  $(\mathcal{S}, \mathcal{A}, \mathcal{T}, \mathcal{R}, \lambda)$ .

**State ( $s$ ) and State Space ( $\mathcal{S}$ ):** We represented a grid of size  $M \times N$  as a matrix of the same shape with the entries corresponding to the game element occupying the position in the grid—p (PacMan), g (Ghost), f (Food), w (Wall), or e (Empty). The state space  $\mathcal{S}$  refers to the set of all possible states.

**Action Space ( $\mathcal{A}(s)$ ):** Set of legal actions PacMan could take in state  $s$ . PacMan can move Left, Right, Up, or Down but not enter walls. Thus, when the PacMan is at the top left position the set of legal actions was only {Right, Down}.

**Transition Matrix ( $\mathcal{T}(s_i, a, s_j)$ ):** Probability of moving to state  $s_j$  if the agent took action  $a$  at state  $s_i$  (Fig. 2a).

**Reward Function ( $\mathcal{R}(s)$ ):** PacMan received +20 for eating a food pellet, -1 for every time step, -200 when it was killed, and +500 for finishing the game. (Cederborg et al. 2015).

**Game Stochasticity:** The motion of PacMan is deterministic—a left action (if legal) will ensure that PacMan moves left. However, ghosts move stochastically according to a prefixed distribution. For instance, a RandomGhost moves in all directions with equal probability (accounting for walls). Thus, the game is nondeterministic.

MDPs for Pong and Breakout are defined analogously. For additional details, please refer to Supplementary Section **Domains**.

### Noise Injection Variation: Generating new controlled environments

We generate controlled variations of an original MDP by explicitly computing its Transition Function and then adding sampled noise to it.

**Explicit enumeration of all states:** States are defined by the position of the game elements. The probability of transitioning from one state to another is computed by multiplying the probability that each game element is able to reach the final configuration independently. Therefore, we visualize the game as a tree, each state is a node, and the edges represent the transition probabilities of the game elements independently reaching their final configuration. By rolling out all possible moves by each game elements at each step, we enumerate all possible reachable states.

**Explicit computation of Transition Function:** Once we have all possible states, we can calculate the transition function, denoted as  $\mathcal{T}(s_i, a, s_j)$ . This function is determined by calculating the probability of each game character moving from one state to another independently.

**Creating  $\delta$ -environments:** We introduce variations in the game environment by modifying the transition function to

$\mathcal{T}_\delta = \mathcal{T} + \delta$ . Here,  $\delta$  is a variable that follows a normal distribution, randomly chosen before each game to add unpredictability (Fig. 2c). The modified transition function,  $\mathcal{T}_\delta$ , is then adjusted to make sure the total probability of moving from any state  $s_i$  using action  $a$  to any other state  $s_j$  sums to 1.

$$\mathcal{T}_\delta(s_j, a, s_i) = \frac{|\mathcal{S}|p_{i,j} + \delta_{i,j}}{|\mathcal{S}| + \sum_j \delta_{i,j}} \quad (4)$$

$|\mathcal{S}|$  denotes the number of states, and guarantees the probability of legal successors does not approach 0 as the state space grows. We investigated two settings—(i) *Low-Noise* with  $\delta \sim \mathcal{N}(0, 0.1)$ , where some non-standard transitions previously impossible without noise are now possible with a low probability. (ii) *High-Noise* with  $\delta \sim \mathcal{N}(0, 0.5)$ , where non-standard transitions are possible with higher probability. We further analyze minimum  $\mathcal{N}(0, 0)$ , and maximum  $\mathcal{N}(0, 1)$  perturbation settings in the Supplement Sec. **Perturbation Bounds**.

## Experimental Details

We compared the mean reward curve of Learnability and Generalization agents. An agent  $\mathcal{G}_T$  is said to generalize well with respect to  $\mathcal{M}_\delta$ , if its mean reward is as good as the corresponding Learnability agent  $\mathcal{L}_\delta$ .

Agents are trained with both tabular Q-Learning (Watkins and Dayan 1992) and SARSA Q-learning (Kaelbling, Littman, and Moore 1996), using Boltzmann or  $\epsilon$ -greedy exploration strategies. In particular, we trained agents for 1,000 episodes and averaged results over 500 trained agents. After every 10 training episodes, agents were evaluated using 10 testing episodes. We report the mean reward curves at convergence. Hyperparameters were inherited from past work (Cederborg et al. 2015) and are available in the Supplement in Sec. **Training Parameters**. We extended the analysis to DQN (Cobbe et al. 2019) and reported the results in the Supplement in Sec. **DQN**. The experiments were conducted on a system with an Intel(R) Xeon(R) CPU E5-2683 v4 @ 2.10GHz.

## Results

We report findings from the Generalization and Learnability agents trained with the multiple variations of PacMan, Pong, and Breakout as described in Sec. **Generating MDPs for investigating generalization** and Table 1.

### Generalization agents can outperform Learnability agents in several instances of the *Indoor-Training Effect*

The mean reward increased with training, as expected, (Fig. 3a), both for the Generalization agent (red) and for the Learnability agent (green). Also, as intuitively expected, both agents performed better under low-noise conditions (solid lines) compared to high-noise conditions (lines with ‘-’ markers). Less intuitive was the relationship between Generalization and Learnability agents. Intriguingly, the Generalization agent consistently outperformed the Learnability

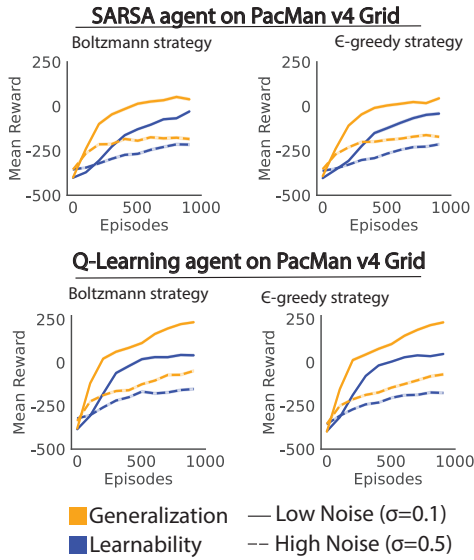


Figure 3: *Generalization agents can outperform Learnability agents.* Results for PacMan v4 grid reporting mean reward as a function of episode number. (a) SARSA agent trained with a Boltzmann exploration strategy for Target MDPs generated with both high (solid line) and low (line with ‘x’ markers) level noise injection. The Generalization Agent (red) beats the Learnability Agent (green) (two-sided t-test,  $p < 0.001$ ). (b) The same result holds for a SARSA agent trained with the  $\epsilon$ -greedy exploration strategy. This finding also holds for Q-Learning agents trained with (c) Boltzmann and (d)  $\epsilon$ -greedy exploration strategies. Standard deviation across the 500 agents is reported as the error bar in all figures. However, the standard deviation is too small for these error bars to be visible.

agent (two-sided t-test,  $p < 0.001$ ). This gap continued until convergence at 1,000 episodes, was observed both across low and high noise levels (solid lines versus ‘-’ lines), when using a Boltzmann strategy (Fig. 3a, c) or an  $\epsilon$ -greedy strategy (Fig. 3b, d), and when using SARSA agents (Fig. 3a, b) or Q-Learning agents (Fig. 3c, d). Another metric commonly used to assess performance is the *Area Under the Curve* (AUC). We compute the ratio between the learnability and generalization agents’ AUC and normalize it using regret. (see Supp. Sec. **Regret Normalization**).

To assess whether this observation was dependent on the target MDP, we replicated these findings on multiple PacMan grids and noise variations (Fig. 4a-f). In (Fig. 4), the Generalization agents beat the Learnability agents, for both low and high levels of noise (see Supp. Sec. **Additional Graphs Non-Semantic Variations**: Figs. Sup3- Sup5 for Boltzmann strategy and Q-learning results).

We also extended these findings to two additional ATARI games, Pong Fig. Sup1 and Breakout Fig. Sup2, to assess their applicability across different games (Fig. 5). Consistent with the results described for Pacman, the Generalization agent was on par with or better than the Learnability agent

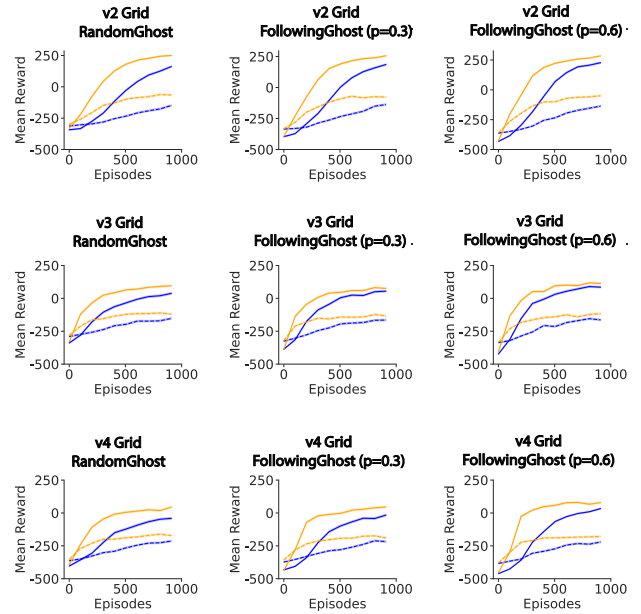


Figure 4: *Generalization can outperform Learnability across multiple variations of PacMan.* Format and conventions as in Fig. 3. (a) Agents trained on the PacMan v2 grid with the Ghost dynamics set to the RandomGhost setting. (b) Agents trained on v2 with a DirectionalGhost with  $p = 0.3$ . (c) DirectionalGhost with  $p = 0.6$ . (d),(e),(f) Variations with the v3 grid with RandomGhost, DirectionGhost ( $p = 0.3$ ) and DirectionalGhost ( $p = 0.6$ ), respectively. All experiments are shown for SARSA agents trained with the  $\epsilon$ -greedy exploration strategy. Generalization agents consistently beat Learnability Agents (two-sided t-test,  $p < 0.001$ ). Corresponding results for agents trained with SARSA + Boltzmann exploration strategy, and for Q-Learning with both  $\epsilon$ -greedy and Boltzmann exploration strategies are shown in Figures Sup3- Sup5.

in Pong Fig. 5a,b) and Breakout Fig. 5c,d) (two-sided t-test,  $p < 0.001$ ; see Figs. Sup6- Sup12 for results with Q-Learning, Sarsa and different sampling strategies).

In sum, there exist several MDPs where it is better to train on a different MDP than the target. These results provide novel intriguing evidence suggesting that training on a different MDP can enable more efficient policy learning than training on the target environment.

### Instances of the *Indoor-Training Effect* in semantic variations of ATARI games

The results presented so far focused on altered MDPs generated by noise injection. Next, we evaluated *semantic* variations, where the changes are more meaningful and interpretable. Specifically, we modified the transition probabilities of Pacman so that ghosts could teleport to new locations, and Pong so that the paddle could follow the ball. We refer to these alternate semantic environments as  $\mathcal{M}_{T'}$  (semantic noise), in contrast to  $\mathcal{M}_{\delta}$  used for noise injection.

For PacMan, Learnability agents were trained and tested

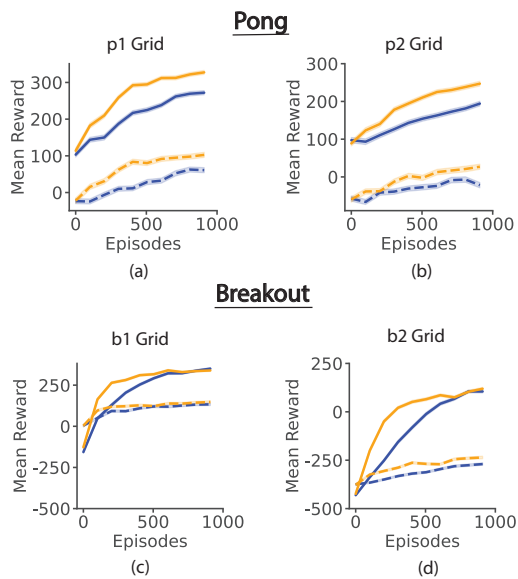


Figure 5: *Generalization agents outperform Learnability agents on Pong and Breakout as well.* Format and conventions as in Fig. 3. Performance of SARSA agents trained with an  $\epsilon$ -greedy exploration strategy on (a) Pong p1 grid, (b) Pong p2 grid, (c) Breakout b1 grid, and (d) Breakout b2 grid. The Generalization Agent consistently beats the Learnability Agent (two-sided t-test,  $p < 0.001$ ).

using TeleportingGhosts ( $\mathcal{M}_{T'}$ ), while the Generalization agents were trained with PacMan with RandomGhosts ( $\mathcal{M}_T$ ) and then tested on TeleportingGhosts ( $\mathcal{M}_{T'}$ ) (Fig. 6a, b, Supp. Sec. **Additional Graphs Non-Semantic Variations**). Even under these semantic noise conditions, Generalization agents outperformed Learnability agents (two-sided t-test,  $p < 0.001$ ; see Figs. Sup13-Sup15 for results with Q-Learning, Sarsa and different sampling strategies). In the case of Pong, we report analogous results with  $\mathcal{M}_{T'}$  set to FollowingPaddle, and  $\mathcal{M}_T$  set to RandomPaddle. Generalization agents also outperformed Learnability agents (by a smaller margin) in both the p1 and p2 grids (Fig. 6c,d). Analogous results for Pong with Q-Learning and other exploration strategies are reported in Figs. Sup16- Sup23.

### The exploration patterns of state-action pairs can predict differences between Generalization and Learning agents

To better understand how Generalization agents could outperform Learnability agents, we investigated the exploration patterns for  $\mathcal{L}_\delta$  and  $\mathcal{G}_T$ . We enumerated all State (S)-Action (A) Pairs, and divided them into three groups—(i) Percentage of S-A pairs explored by both agents ( $P_{LG}$ ), (ii) Percentage of pairs explored only by the Learnability agent ( $P_L$ ), and (iii) Percentage of pairs explored only by the Generalization agent ( $P_G$ ). Thus,  $P_{LG} + P_L + P_G = 100$ . We defined  $D_{LG} = P_L + P_G$ , the divergence in the exploration patterns between these two agents.

In Fig. 7 we visualize  $D_{LG}$  for grids where  $\mathcal{G}_T$  outper-

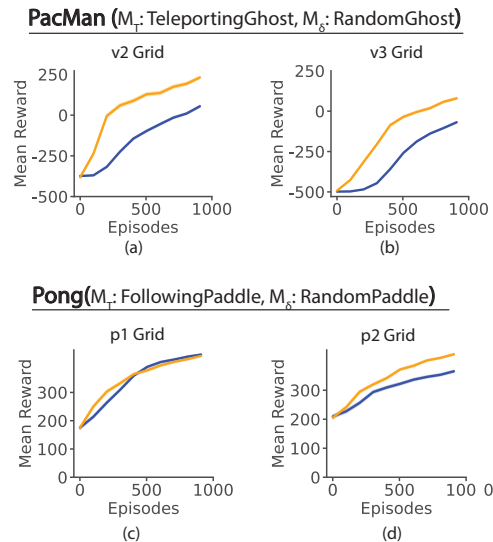


Figure 6: *Generalization agents outperform Learnability agents on semantic variations of PacMan and Pong as well.* Format and conventions as in Fig. 3. (a) Given the target PacMan MDP with the v2 grid and TeleportingGhost, the Generalization trained on the RandomGhost outperformed the Learnability agent that was trained and tested on the same Target MDP (TeleportingGhost) (two-sided t-test,  $p < 0.001$ ). (b) This finding extends to TeleportingGhost and RandomGhost MDPs with the PacMan v3 Grid as well. (c) For the Pong p1 grid, Generalization agents trained on an MDP with DirectionalPaddle performed better on the RandomPaddle MDP during testing, as compared to the Learnability Agent trained and tested on the RandomPaddle MDP. (d) The same finding extends to the p2 grid as well.

formed  $\mathcal{L}_\delta$  agents and compare it to cases where it did not. Fig. 7a shows an agent trained with Q-Learning and Boltzmann exploration strategy for the Pacman v3 grid with RandomGhost stochasticity, where  $\mathcal{G}_T$  beat the  $\mathcal{L}_\delta$  agent. The corresponding panel Fig. 7b depicts  $D_{LG}$ —each entry of this grid represents an S-A pair. We refer to this plot as the *exploration grid* for these agents. The exploration grid shows that most S-A pairs were explored by both agents, with almost no pairs explored only by one type of agent and therefore no significant differences in their exploration patterns. In contrast, Fig. 7c, d report S-A pairs for PacMan v2, here the  $\mathcal{G}_T$  agent performs worse than the  $\mathcal{L}_\delta$  agent. The exploration grid reveals that there is a high fraction of S-A pairs explored either by one *or* the other agent but not both.

We grouped all the cases where  $\mathcal{L}_\delta > \mathcal{G}_T$  ( Fig. 7e, brown) and all the cases where  $\mathcal{L}_\delta < \mathcal{G}_T$  ( Fig. 7e, gray) and computed  $D_{LG}$ . On average,  $D_{LG}$  was significantly higher in MDPs where  $\mathcal{L}_\delta > \mathcal{G}_T$  (two-sided t-test,  $p < 0.05$ ). The same result holds true for Pong MDPs as reported in Fig. 7f. Exploration grids and additional results for variations of PacMan (Sup25-Sup32), Pong (Sup33-Sup40), and Breakout (Sup41-Sup44) can be found in the Supplement in Sec. **Additional Graphs State-Action Pairs**. Instead of grouping

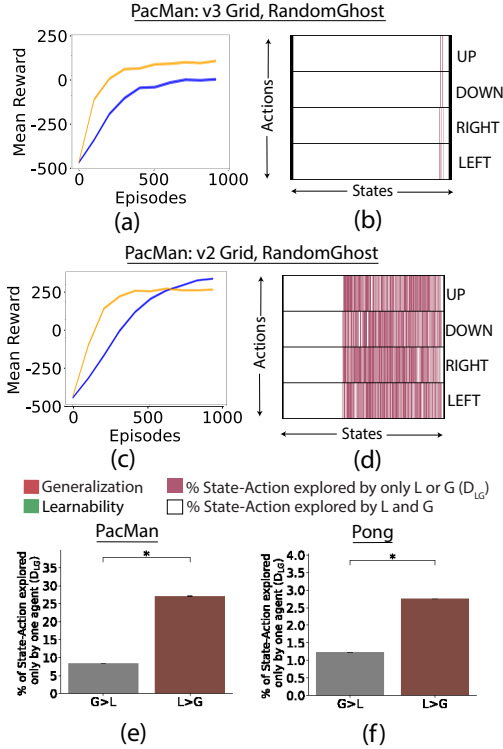


Figure 7: *The exploration patterns predict the reward gap between  $\mathcal{L}_\delta$  and  $\mathcal{G}_T$ .* (a) Reward for agents trained on Pacman v3, where  $\mathcal{G}_T$  outperforms  $\mathcal{L}_\delta$  (format as in Fig. 3). (b) Exploration grid visualizing the difference in State-Action ( $\mathcal{S}$ - $\mathcal{A}$ ) pairs explored by these agents ( $D_{LG}$ ). The grid shows States on the x-axis and Actions on the y-axis. The black lines separate the Actions for clarity. Each cell corresponds to one  $\mathcal{S}$ - $\mathcal{A}$  pair. In this case, a negligible fraction of  $\mathcal{S}$ - $\mathcal{A}$  pairs were visited only by one agent (pink). (c) Rewards for agents trained on PacMan v3. Here,  $\mathcal{G}_T$  performs worse than  $\mathcal{L}_\delta$  at the end of training. (d) A large fraction of pairs were only visited by either one or the other agent but not both (contrast with part (b)). (e)  $D_{LG}$  averaged over PacMan grids where  $\mathcal{G}_T$  outperformed  $\mathcal{L}_\delta$  (gray) and vice-versa (brown). (f)  $D_{LG}$  averaged over Pong grids. The "\*" is for statistical significance (two-sided t-test,  $p < 0.001$ ).

MDPs, we also conducted a correlation analysis. We defined the Reward Gap:  $R_{LG} = R_G - R_L$ . The Spearman correlation coefficient between  $D_{LG}$  and  $R_{LG}$  was 0.43 ( $p < 0.005$ ) for PacMan and 0.26 ( $p < 0.005$ ) for Pong. Combined, these analyses show that the *Indoor-Training Effect* is associated with similar exploration patterns in the training and testing environments.

## Discussion

In this work, our objective is to understand the paradoxical *Indoor-Training Effect* - where agents perform better when trained in a noise-free environment and tested in noisy  $\delta$ -environments, compared to being trained and tested in the same  $\delta$ -environments. Similarly to how training in a quiet,

noise-free indoor environment helps athletes focus on mastering the fundamentals of tennis, we explore whether training in certain environments is more conducive to learning than training on the same testing environment.

To investigate this, we propose a new methodology to generate modified MDPs from a given MDP, along with a metric to quantify the distance between different environments. We demonstrate the Indoor-Training Effect across various algorithms and exploration strategies (Fig. 3), grid layouts and game stochasticity (Fig. 4), and multiple ATARI games (Fig. 5). We also showed that this phenomenon extends beyond Noise Injected environments, and can also occur when semantic changes are introduced in the game elements (Fig. 6).

To gain deeper insights into these environments, we examine the exploration patterns of agents under different transition probabilities. Similarly to a tennis player who has never encountered a smash serve during their training and develops an optimal playing style that does not anticipate or respond to such powerful shots, the suboptimal performance of the agents could be caused by a divergence in exploration patterns. We show that the performance gap between agents is indeed correlated with their exploration patterns under different transition probabilities (Fig. 7).

The Indoor-Training Effect is particularly relevant to robotics, where robots often operate in complex, dynamic environments. The Indoor-Training Effect opens new avenues of research, whereby robotic systems could be trained in simplified, controlled settings to master essential skills without the interference of noise. This finding could also enhance their ability to adapt and perform in real-world conditions where unpredictability and noise are prevalent. Such training strategies could lead to more robust, adaptable robots capable of navigating and executing tasks effectively in diverse and challenging environments.

We note that these findings are reminiscent of results with biological agents. For example, recent experiments with the *C. Elegans* worm have shown that biological agents perform best when cross-trained on different environments as compared to being tested on the environments they were trained on (Li, Kreiman, and Ramanathan 2024).

Despite the evidence provided in this study, we would like to highlight two main limitations. Firstly, our experiments were conducted solely in the context of ATARI games. We hope that future research can extend and examine the findings in real-world environments. Secondly, it will be interesting to assess whether the conclusions drawn from classical Reinforcement Learning methods extend to deep RL approaches.

These findings raise fundamental questions about our understanding of RL algorithms. Typically, RL practitioners have strived to train agents in environments that closely resemble their deployment conditions. This approach assumes that matching the training and testing environments is critical for optimal performance. However, the Indoor-Training Effect challenges this assumption by showing that agents trained in noise-free, controlled environments can sometimes outperform those trained in more chaotic, realistic settings when faced with noisy, unpredictable scenarios during testing.

## References

- Ahmed, O.; Träuble, F.; Goyal, A.; Neitz, A.; Wüthrich, M.; Bengio, Y.; Schölkopf, B.; and Bauer, S. 2020. CausalWorld: A Robotic Manipulation Benchmark for Causal Structure and Transfer Learning. *CoRR*, abs/2010.04296.
- Bapst, V.; Sanchez-Gonzalez, A.; Doersch, C.; Stachenfeld, K. L.; Kohli, P.; Battaglia, P. W.; and Hamrick, J. B. 2019. Structured agents for physical construction. *CoRR*, abs/1904.03177.
- Barbu, A.; Mayo, D.; Alverio, J.; Luo, W.; Wang, C.; Gutfreund, D.; Tenenbaum, J.; and Katz, B. 2019. Objectnet: A large-scale bias-controlled dataset for pushing the limits of object recognition models. *Advances in neural information processing systems*, 32.
- Bäuerle, N.; and Glauner, A. 2022. Distributionally robust Markov decision processes and their connection to risk measures. *Mathematics of Operations Research*, 47(3): 1757–1780.
- Biedenkapp, A.; Bozkurt, H. F.; Eimer, T.; Hutter, F.; and Lindauer, M. 2020. Dynamic Algorithm Configuration: Foundation of a New Meta-Algorithmic Framework. In *Proceedings of the Twenty-fourth European Conference on Artificial Intelligence (ECAI'20)*.
- Bomatter, P.; Zhang, M.; Karev, D.; Madan, S.; Tseng, C.; and Kreiman, G. 2021. When Pigs Fly: Contextual Reasoning in Synthetic and Natural Scenes. arXiv:2104.02215.
- Cederborg, T.; Grover, I.; Isbell, C. L.; and Thomaz, A. L. 2015. Policy Shaping with Human Teachers. In *International Joint Conference on Artificial Intelligence*.
- Cobbe, K.; Hesse, C.; Hilton, J.; and Schulman, J. 2020. Leveraging Procedural Generation to Benchmark Reinforcement Learning. arXiv:1912.01588.
- Cobbe, K.; Klimov, O.; Hesse, C.; Kim, T.; and Schulman, J. 2019. Quantifying generalization in reinforcement learning. In *International conference on machine learning*, 1282–1289. PMLR.
- DeNero, J.; Klein, D.; and Abbeel, P. 2014. CS188: Berkeley Pacman Projects. <http://ai.berkeley.edu/home.html> (Spring 2014).
- Devin, C.; Abbeel, P.; Darrell, T.; and Levine, S. 2018. Deep object-centric representations for generalizable robot learning. In *2018 IEEE International Conference on Robotics and Automation (ICRA)*, 7111–7118. IEEE.
- Dulac-Arnold, G.; Mankowitz, D. J.; and Hester, T. 2019. Challenges of Real-World Reinforcement Learning. *CoRR*, abs/1904.12901.
- Filos, A.; Tigas, P.; McAllister, R.; Rhinehart, N.; Levine, S.; and Gal, Y. 2020. Can Autonomous Vehicles Identify, Recover From, and Adapt to Distribution Shifts? *CoRR*, abs/2006.14911.
- Geirhos, R.; Rubisch, P.; Michaelis, C.; Bethge, M.; Wichmann, F. A.; and Brendel, W. 2018. ImageNet-trained CNNs are biased towards texture; increasing shape bias improves accuracy and robustness. *arXiv preprint arXiv:1811.12231*.
- Gopalan, N.; Littman, M.; MacGlashan, J.; Squire, S.; Tellex, S.; Winder, J.; Wong, L.; et al. 2017. Planning with abstract Markov decision processes. In *Proceedings of the International Conference on Automated Planning and Scheduling*, volume 27, 480–488.
- Goyal, V.; and Grand-Clement, J. 2023. Robust Markov decision processes: Beyond rectangularity. *Mathematics of Operations Research*, 48(1): 203–226.
- Guss, W. H.; Codel, C.; Hofmann, K.; Houghton, B.; Kuno, N.; Milani, S.; Mohanty, S.; Liebana, D. P.; Salakhutdinov, R.; Topin, N.; et al. 2019. The MineRL 2019 competition on sample efficient reinforcement learning using human priors. *arXiv preprint arXiv:1904.10079*.
- Hafner, D. 2021. Benchmarking the Spectrum of Agent Capabilities. *CoRR*, abs/2109.06780.
- Justesen, N.; Torrado, R. R.; Bontrager, P.; Khalifa, A.; Torgelius, J.; and Risi, S. 2018. Illuminating generalization in deep reinforcement learning through procedural level generation. *arXiv preprint arXiv:1806.10729*.
- Kaelbling, L. P.; Littman, M. L.; and Moore, A. W. 1996. Reinforcement Learning: A Survey. *J. Artif. Intell. Res.*, 4: 237–285.
- Kang, K.; Belkhale, S.; Kahn, G.; Abbeel, P.; and Levine, S. 2019. Generalization through simulation: Integrating simulated and real data into deep reinforcement learning for vision-based autonomous flight. In *2019 international conference on robotics and automation (ICRA)*, 6008–6014. IEEE.
- Kirk, R.; Zhang, A.; Grefenstette, E.; and Rocktäschel, T. 2021. A Survey of Generalisation in Deep Reinforcement Learning. *CoRR*, abs/2111.09794.
- Li, C.; Kreiman, G.; and Ramanathan, S. 2024. Discovering neural policies to drive behavior by integrating deep reinforcement learning agents with biological neural networks. *Nature Machine Intelligence*, In Press.
- Lyle, C.; Rowland, M.; Dabney, W.; Kwiatkowska, M.; and Gal, Y. 2022. Learning dynamics and generalization in deep reinforcement learning. In *International Conference on Machine Learning*, 14560–14581. PMLR.
- Madan, S.; Henry, T.; Dozier, J.; Ho, H.; Bhandari, N.; Sasaki, T.; Durand, F.; Pfister, H.; and Boix, X. 2022a. When and how convolutional neural networks generalize to out-of-distribution category–viewpoint combinations. *Nature Machine Intelligence*, 4(2): 146–153.
- Madan, S.; Sasaki, T.; Pfister, H.; Li, T.-M.; and Boix, X. 2023. Adversarial examples within the training distribution: A widespread challenge. arXiv:2106.16198.
- Madan, S.; You, L.; Zhang, M.; Pfister, H.; and Kreiman, G. 2022b. What makes domain generalization hard? arXiv:2206.07802.
- Michaelis, C.; Mitzkus, B.; Geirhos, R.; Rusak, E.; Bringmann, O.; Ecker, A. S.; Bethge, M.; and Brendel, W. 2019. Benchmarking robustness in object detection: Autonomous driving when winter is coming. *arXiv preprint arXiv:1907.07484*.
- Mondal, S. S.; Dulberg, Z.; and Cohen, J. 2022. Generalization to Out-of-Distribution transformations.

Moos, J.; Hansel, K.; Abdulsamad, H.; Stark, S.; Clever, D.; and Peters, J. 2022a. Robust Reinforcement Learning: A Review of Foundations and Recent Advances. *Machine Learning and Knowledge Extraction*, 4(1): 276–315.

Moos, J.; Hansel, K.; Abdulsamad, H.; Stark, S.; Clever, D.; and Peters, J. 2022b. Robust reinforcement learning: A review of foundations and recent advances. *Machine Learning and Knowledge Extraction*, 4(1): 276–315.

Nilim, A.; and El Ghaoui, L. 2005. Robust control of Markov decision processes with uncertain transition matrices. *Operations Research*, 53(5): 780–798.

OpenAI; Akkaya, I.; Andrychowicz, M.; Chociej, M.; Litwin, M.; McGrew, B.; Petron, A.; Paino, A.; Plappert, M.; Powell, G.; Ribas, R.; Schneider, J.; Tezak, N.; Tworek, J.; Welinder, P.; Weng, L.; Yuan, Q.; Zaremba, W.; and Zhang, L. 2019. Solving Rubik’s Cube with a Robot Hand. *CoRR*, abs/1910.07113.

Osiński, B.; Jakubowski, A.; Zięcina, P.; Miłoś, P.; Galias, C.; Homoceanu, S.; and Michalewski, H. 2020. Simulation-based reinforcement learning for real-world autonomous driving. In *2020 IEEE International Conference on Robotics and Automation (ICRA)*, 6411–6418. IEEE.

Packer, C.; Gao, K.; Kos, J.; Krähenbühl, P.; Koltun, V.; and Song, D. 2018. Assessing generalization in deep reinforcement learning. *arXiv preprint arXiv:1810.12282*.

Rummery, G. A.; and Niranjan, M. 1994. *On-line Q-learning using connectionist systems*, volume 37. University of Cambridge, Department of Engineering Cambridge, UK.

Sakai, A.; Sunagawa, T.; Madan, S.; Suzuki, K.; Katoh, T.; Kobashi, H.; Pfister, H.; Sinha, P.; Boix, X.; and Sasaki, T. 2022. Three approaches to facilitate invariant neurons and generalization to out-of-distribution orientations and illuminations. *Neural Networks*, 155: 119–143.

Squire, S.; Tellex, S.; Arumugam, D.; and Yang, L. 2015. Grounding English commands to reward functions. In *Robotics: Science and Systems*.

Stone, A.; Ramirez, O.; Konolige, K.; and Jonschkowski, R. 2021. The Distracting Control Suite – A Challenging Benchmark for Reinforcement Learning from Pixels. *arXiv:2101.02722*.

Tellex, S.; Kollar, T.; Dickerson, S.; Walter, M.; Banerjee, A.; Teller, S.; and Roy, N. 2011. Understanding natural language commands for robotic navigation and mobile manipulation. In *Proceedings of the AAAI Conference on Artificial Intelligence*, volume 25, 1507–1514.

Walter, M. R.; Hemachandra, S. M.; Homberg, B. S.; Tellex, S.; and Teller, S. 2013. Learning semantic maps from natural language descriptions. *Robotics: Science and Systems*.

Watkins, C. J. C. H.; and Dayan, P. 1992. Q-learning. *Machine Learning*, 8(3): 279–292.

Zhu, Y.; Wong, J.; Mandlekar, A.; and Martín-Martín, R. 2020. robosuite: A Modular Simulation Framework and Benchmark for Robot Learning. *CoRR*, abs/2009.12293.

Zhu, Z.; Lin, K.; Jain, A. K.; and Zhou, J. 2023. Transfer learning in deep reinforcement learning: A survey. *IEEE Transactions on Pattern Analysis and Machine Intelligence*.

## Reproducibility Checklist

- **Includes a conceptual outline and/or pseudocode description of AI methods introduced:** Yes (preliminaries: Reinforcement Learning)
- **Clearly delineates statements that are opinions, hypothesis, and speculation from objective facts and results:** Yes (Introduction, Results)
- **Provides well-marked pedagogical references for less-familiar readers to gain background necessary to replicate the paper:** Yes (Preliminaries, Related Works)
- **Does this paper make theoretical contributions?** No
- **Does this paper rely on one or more datasets?** No
- **Does this paper include computational experiments?** Yes (Experimental Details)

If yes, please complete the list below.

- **Any code required for pre-processing data is included in the appendix:** Yes (Code Availability)
- **All source code required for conducting and analyzing the experiments is included in a code appendix:** Yes (Code Availability)
- **All source code required for conducting and analyzing the experiments will be made publicly available upon publication of the paper with a license that allows free usage for research purposes:** Yes (Code Availability)
- **All source code implementing new methods have comments detailing the implementation, with references to the paper where each step comes from:** Yes (Code Availability)
- **If an algorithm depends on randomness, then the method used for setting seeds is described in a way sufficient to allow replication of results:** Yes (Experimental Details)
- **This paper specifies the computing infrastructure used for running experiments (hardware and software), including GPU/CPU models; amount of memory; operating system; names and versions of relevant software libraries and frameworks:** Yes (Experimental Details)
- **This paper formally describes evaluation metrics used and explains the motivation for choosing these metrics:** Yes (Experimental Details)
- **This paper states the number of algorithm runs used to compute each reported result:** Yes (Experimental Details)
- **Analysis of experiments goes beyond single-dimensional summaries of performance (e.g., average; median) to include measures of variation, confidence, or other distributional information:** Yes (Results)
- **The significance of any improvement or decrease in performance is judged using appropriate statistical tests (e.g., Wilcoxon signed-rank):** Yes (Results)
- **This paper lists all final (hyper-)parameters used for each model/algorithm in the paper's experiments:** Yes (Experimental Details, Supplement)

- **This paper states the number and range of values tried per (hyper-) parameter during development of the paper, along with the criterion used for selecting the final parameter setting:** Yes (Experimental Details, Supplement)

## Appendix

### Domains

We present details for the ATARI PacMan, Pong and Breakout domains.

#### PacMan

PacMan is set in a two-dimensional grid that contains food, walls, ghosts, and the PacMan character. The game concludes with a +500 reward when all food pellets are consumed, while encountering a ghost results in a -500 penalty and game over. Each consumed food pellet awards +10 points, and PacMan incurs a -1 penalty for every time step. The available actions for PacMan are moving Up, Down, Right, or Left. The game’s state includes the location of PacMan, the position and direction of any ghosts, and the distribution of food pellets. In this iteration of the game, ghosts move according to some distributions.

#### Pong

In this one-player version of Pong, the player competes against a computer-controlled paddle. The game is set on a two-dimensional grid, with the player controlling one paddle and the computer controlling the other. The game concludes with a +500 reward when the ball reaches the grid boundaries on the computer controlled paddle side, while if the grid boundary is reached on the agent’s side, a -500 penalty is applied and game over. The agent incurs a -1 penalty for every time step. The available actions for the paddles are moving Right and Left or to Stop. The game’s state includes the location of the ball and the position and direction of any paddle. In this iteration of the game, the computer controlled paddle moves according to some distribution. Visualizations of the grids are presented in Sup1.

#### Breakout

In this version of Breakout, the agent competes against a wall of bricks using a horizontally-moving paddle and a ball. The game is set on a two-dimensional grid, with the agent controlling the paddle located at the bottom of the screen. The objective is to break bricks by hitting them with the ball, which bounces back after each hit. The game concludes with a +500 reward when all bricks are destroyed, but if the ball passes the paddle and reaches the bottom grid boundary, a -500 penalty is applied, resulting in game over. Each hit brick awards +10 points, and the agent incurs a -1 penalty for every time step. The available actions for the agent’s paddle are moving Right or Left, or choosing to Stop. The game’s state includes the position of the ball, the location of the paddle, and the configuration and status of the bricks. Visualizations of the grids are presented in Sup2.

### Training Parameters

In our experiments, the parameters for Q-Learning and SARSA are inherited by (Cederborg et al. 2015). In particular,  $T = 1.5$ ,  $\alpha = 0.05$ , and  $\lambda = 0.9$ .

### Additional Graphs Non-Semantic Variations

In this section we present supplementary results showing the Generalization Agent and Learnability Agent behavior for Semantic variations of grids throughout Pacman and Pong.

#### PacMan

Additional results showing the Generalization Agent and Learnability Agent behaviour in Pacman for grids  $v2$ ,  $v3$ ,  $v4$ , are presented in the Supplementary figures. In particular, results for SARSA Agent with Boltzmann exploration strategy are presented in Sup3. Sup4, Sup5 show Q-learning Agent with Boltzmann and  $\epsilon$ -greedy exploration strategies respectively.

#### Pong

Similarly, for Pong grids  $p1$ ,  $p2$  results are presented in the Supplementary figures Sup6 for SARSA Agent and Sup7, Sup8 for Q-learning Agent.

#### Breakout

Analogously, for Breakout grids  $b1$ ,  $b2$ ,  $b3$  results are presented in the Supplementary figures Sup9, Sup10 for SARSA Agent and Sup11, Sup12 for Q-learning Agent.

### Additional Graphs Semantic variations

In this section we present supplementary results showing the Generalization Agent and Learnability Agent behavior for Semantic variations of grids throughout Pacman and Pong.

#### PacMan

The behavior of the Generalization and Learnability Agents under semantic variations of PacMan on grids  $v2$ ,  $v3$ ,  $v4$  are presented in Supplementary figures Sup13 for SARSA Agent and Sup14 and Sup15 for Q-learning Agent.

#### Pong

Similarly, for Pong grids  $p1$ ,  $p2$  results are presented in the Supplementary figures. In particular, semantic variations featuring Directional Ghost  $p = 0.3$  are presented in Sup16, Sup17 for SARSA Agent and Sup18, Sup19 for Q-learning Agent. While semantic variations featuring Directional Ghost  $p = 0.6$  are shown in Sup22, Sup21 for SARSA Agent and Sup24, Sup23 for Q-learning.

### Additional Graphs State-Action Pairs

This section shows the supplementary results for the *exploration grid* visualizing the difference in State-Action (S-A) pairs explored by these agents ( $D_{LG}$ ) throughout the analyzed domains.

#### PacMan

Results of the *exploration grid* for PacMan  $v2$ ,  $v3$ ,  $v4$  are shown in Supplementary figures. In particular, for non-semantic grid variations, Sup25 and Sup26 report grid exploration graphs for Q-learning Agent and Sup27 and Sup28 for SARSA Agent. Additionally, for semantic games variations, Sup29 and Sup30 report grid exploration graphs for Q-learning Agent and Sup31 and Sup32 for SARSA Agent.

## Pong

Similarly, for pong  $p1$  and  $p2$ , Sup33, Sup34, Sup35, and Sup36 report grid exploration graphs for non-semantic variations of Q-learning Agent and SARSA Agent respectively, while Sup37, Sup38, Sup39, and Sup40 for semantic variations.

## Breakout

For Breakout grids  $b1, b2$ , and  $b3$ , exploration graphs for non-semantic variations of Q-learning Agent and SARSA Agent are reported in Supplementary figures Sup41, Sup42, Sup43, and Sup44.

## Regret Normalization

*Regret* quantifies the performance gap between an agent’s actions and the optimal actions it could have taken. Specifically, it measures the loss incurred due to suboptimal decisions compared to a theoretical best-case scenario. We take the ratio of the learnability and generalization agents’ regrets in an effort to provide normalized AUC measures for both non-semantic (Sup45) and semantic (Sup46) game variations of Pac Man ( $v1, v2, v3$ ) and Pong ( $p1, p2$ ).

## DQN

To address the generalizability of the Indoor-Training Effect to deep learning-based methods, we extended our experiments to include DQN, a widely used deep reinforcement learning algorithm. The results, reported in the appendix, demonstrate the consistency of our findings with DQN as shown in Sup47 for non-semantic variations of Pac Man’s grids  $v1, v2, v3$  and Sup48 for semantic variations of the same grids. In particular, we trained agents for 10,000 episodes and averaged results over 50 trained agents. After every 100 training episodes, agents were evaluated using 10 testing episodes. We report the mean reward curves at convergence.

## Perturbation Bounds

We include additional graphs illustrating the performance bounds under maximum and minimum perturbation settings. Specifically, we tested agents in the extreme scenarios of no noise ( $\delta \sim \mathcal{N}(0, 0)$ ) and maximum noise ( $\delta \sim \mathcal{N}(0, 1)$ ) and visualize it with the learnability and generalization agents under the Low-Noise regime. Results across the different agents are reported in Sup49, Sup50, Sup51

## Pong

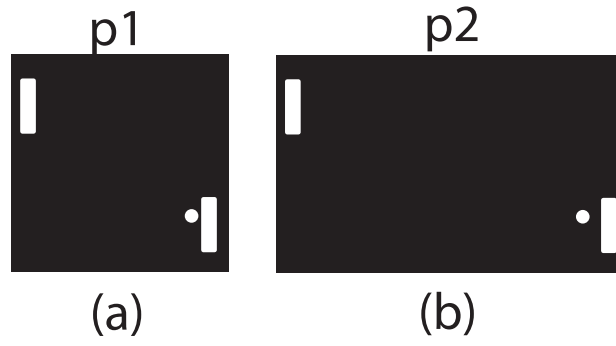


Figure Sup1: *Grid variations for Pong.*

## Breakout

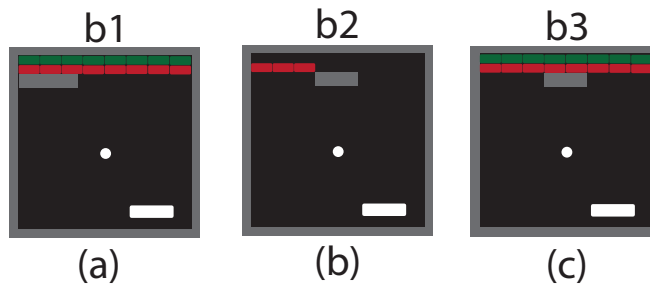


Figure Sup2: *Grid variations for Breakout.*

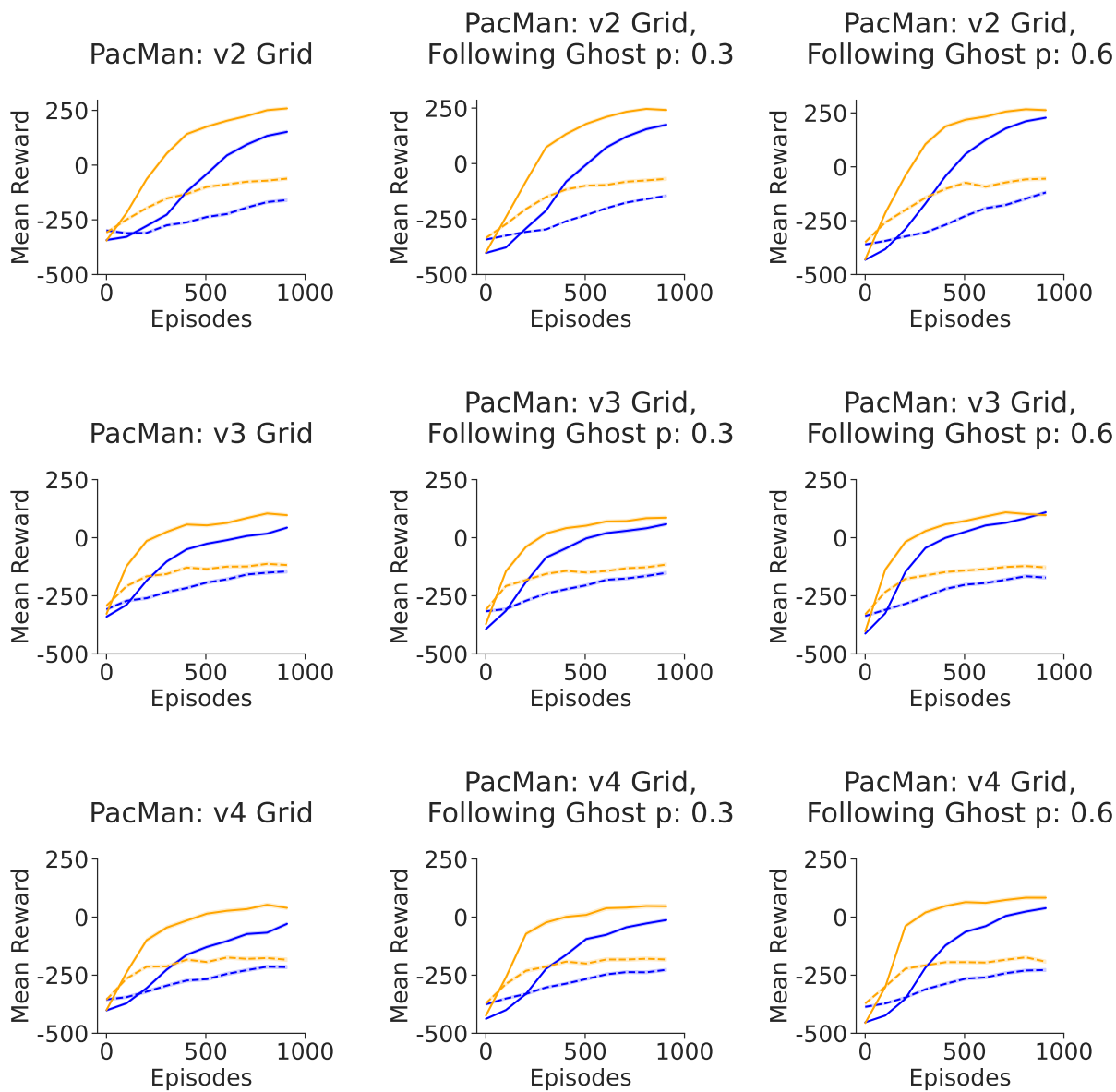


Figure Sup3: *SARSA Agent with Boltzmann exploration strategy*: Results for PacMan v2, v3, v4 grids reporting mean reward as a function of episode number. The agent is trained on the non-noisy version of the environment and tested on different level of noise ( $\delta \sim \mathcal{N}(0, 0.1)$  in Low-Noise and  $\delta \sim \mathcal{N}(0, 0.5)$  in High-Noise settings).

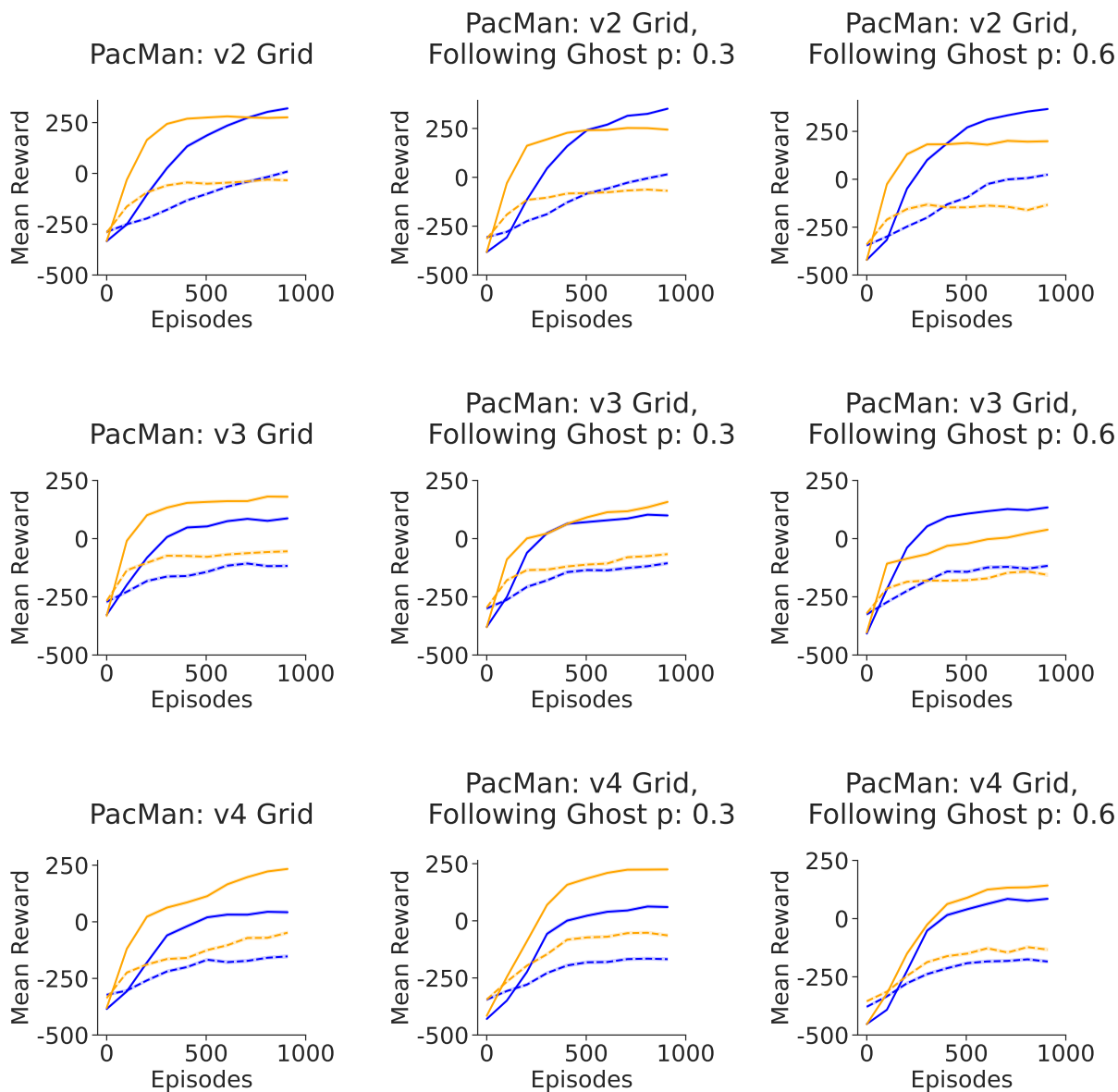


Figure Sup4: *Q-learning Agent with Boltzmann exploration strategy*: Results for PacMan v2, v3, v4 grids reporting mean reward as a function of episode number. The agent is trained on the non-noisy version of the environment and tested on different level of noise ( $\delta \sim \mathcal{N}(0, 0.1)$  in Low-Noise and  $\delta \sim \mathcal{N}(0, 0.5)$  in High-Noise settings).

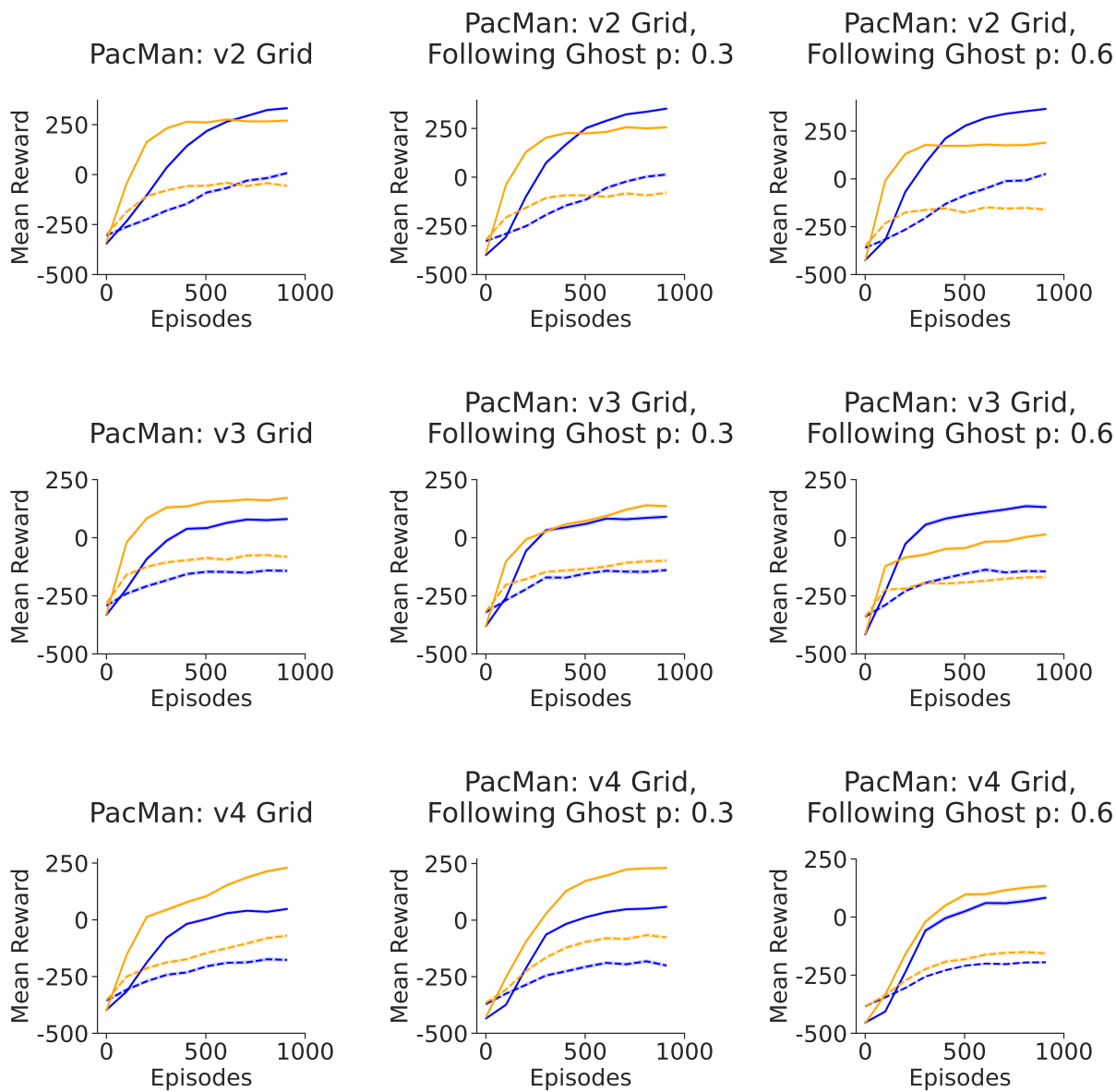


Figure Sup5: *Q-learning Agent with  $\epsilon$ -greedy exploration strategy*: Results for PacMan v2, v3, v4 grids reporting mean reward as a function of episode number. The agent is trained on the non-noisy version of the environment and tested on different level of noise ( $\delta \sim \mathcal{N}(0, 0.1)$  in Low-Noise and  $\delta \sim \mathcal{N}(0, 0.5)$  in High-Noise settings).

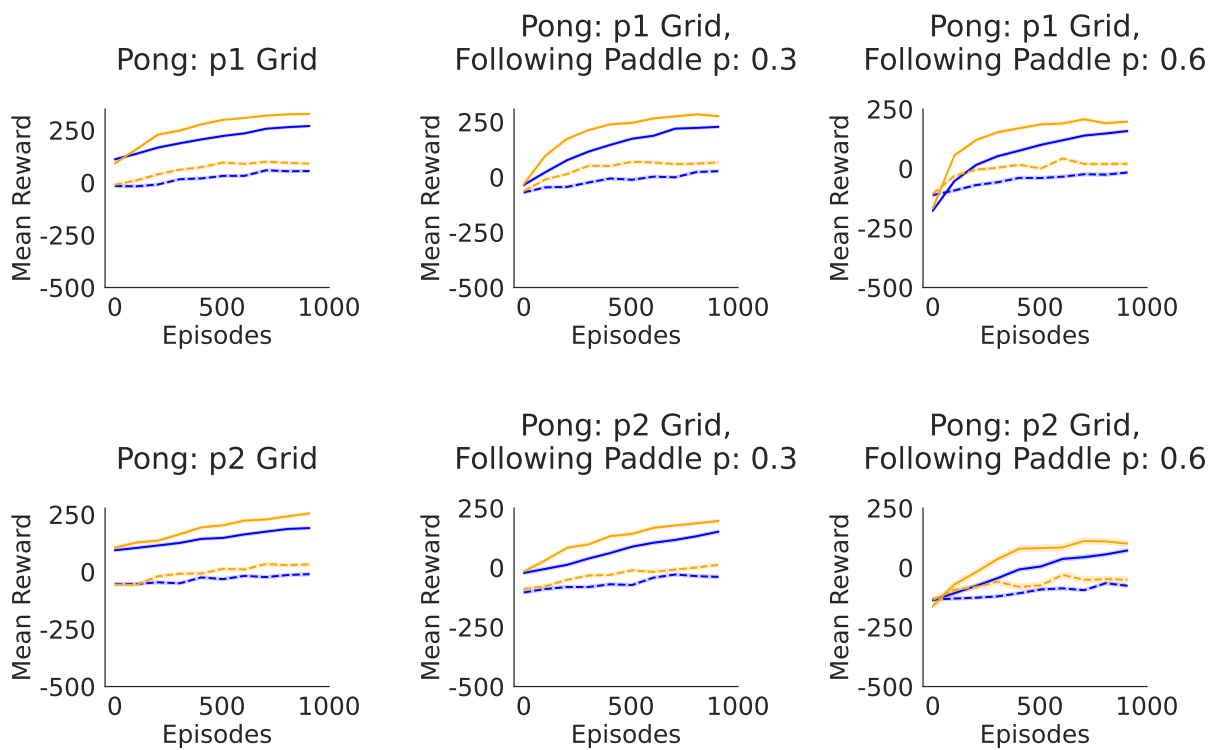


Figure Sup6: *SARSA Agent with Boltzmann exploration strategy*: Results for Pong p1, p2 grids reporting mean reward as a function of episode number. The agent is trained on the non-noisy version of the environment and tested on different level of noise ( $\delta \sim \mathcal{N}(0, 0.1)$  in Low-Noise and  $\delta \sim \mathcal{N}(0, 0.5)$  in High-Noise settings).

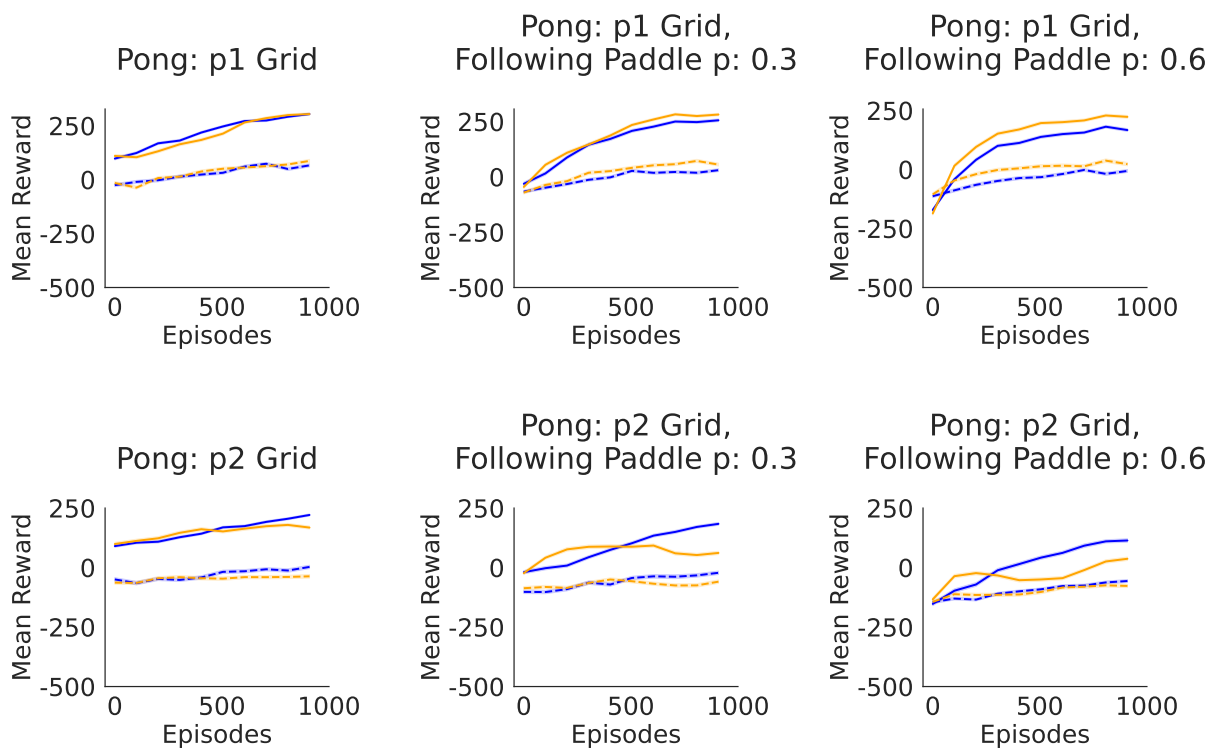


Figure Sup7: *Q-learning Agent with Boltzmann exploration strategy*: Results for Pong p1, p2 grids reporting mean reward as a function of episode number. The agent is trained on the non-noisy version of the environment and tested on different level of noise ( $\delta \sim \mathcal{N}(0, 0.1)$  in Low-Noise and  $\delta \sim \mathcal{N}(0, 0.5)$  in High-Noise settings).

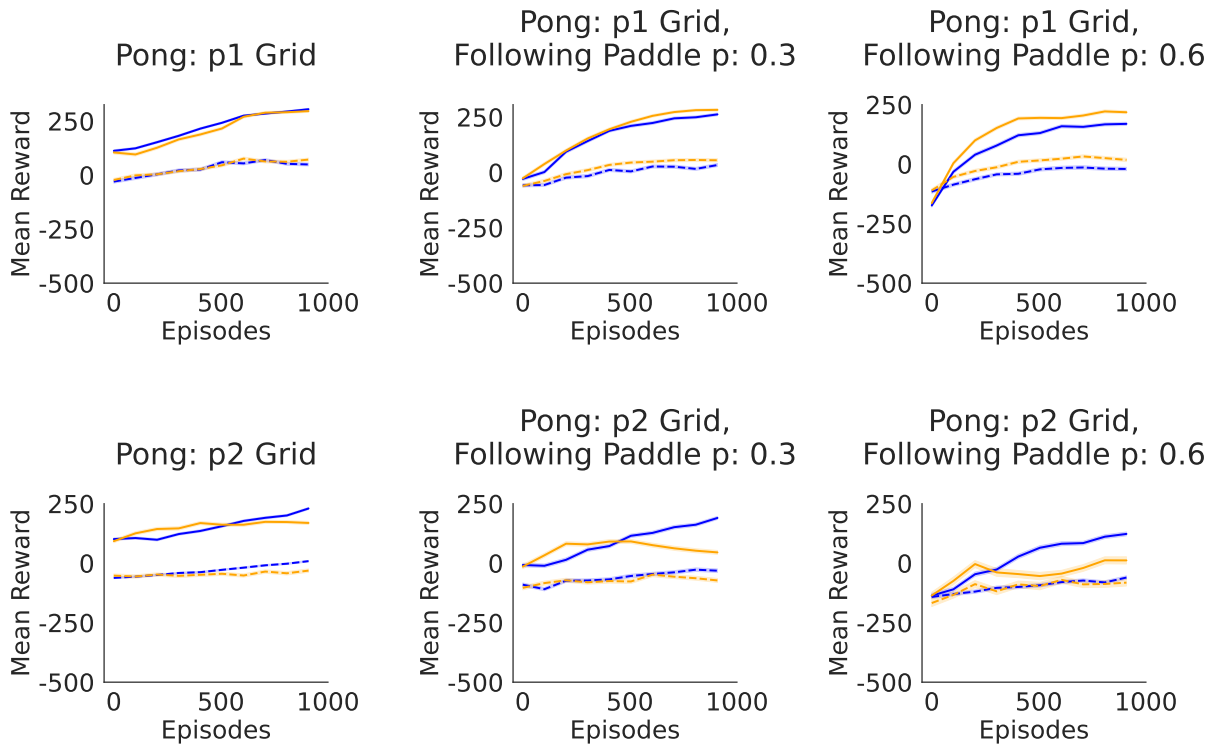


Figure Sup8: *Q-learning Agent with  $\epsilon$ -greedy exploration strategy*: Results for Pong p1, p2 grids reporting mean reward as a function of episode number. The agent is trained on the non-noisy version of the environment and tested on different level of noise ( $\delta \sim \mathcal{N}(0, 0.1)$  in Low-Noise and  $\delta \sim \mathcal{N}(0, 0.5)$  in High-Noise settings).

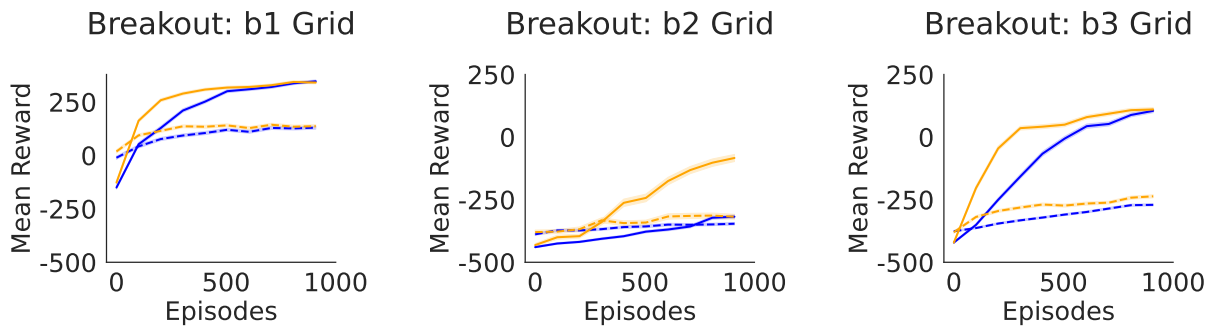


Figure Sup9: *SARSA Agent with Boltzmann exploration strategy*: Results for Breakout b1, b2, b3 grids reporting mean reward as a function of episode number. The agent is trained on the non-noisy version of the environment and tested on different level of noise ( $\delta \sim \mathcal{N}(0, 0.1)$  in Low-Noise and  $\delta \sim \mathcal{N}(0, 0.5)$  in High-Noise settings).

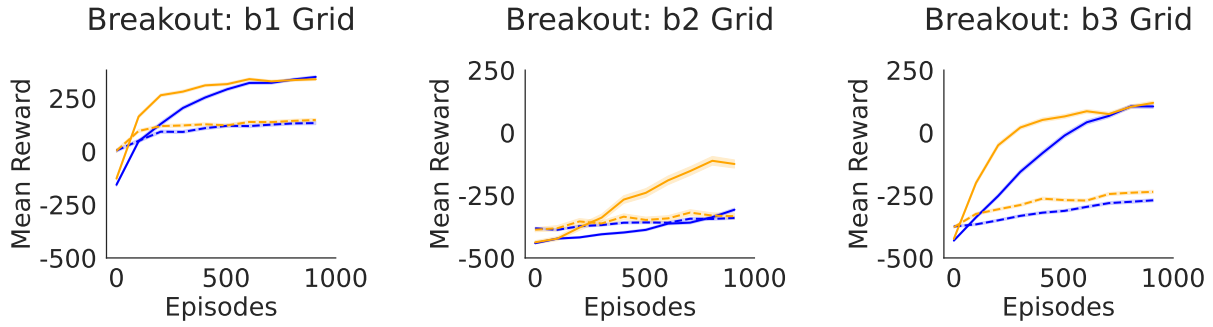


Figure Sup10: *SARSA Agent with  $\epsilon$ -greedy exploration strategy*: Results for Breakout b1, b2, b3 grids reporting mean reward as a function of episode number. The agent is trained on the non-noisy version of the environment and tested on different level of noise ( $\delta \sim \mathcal{N}(0, 0.1)$  in Low-Noise and  $\delta \sim \mathcal{N}(0, 0.5)$  in High-Noise settings).

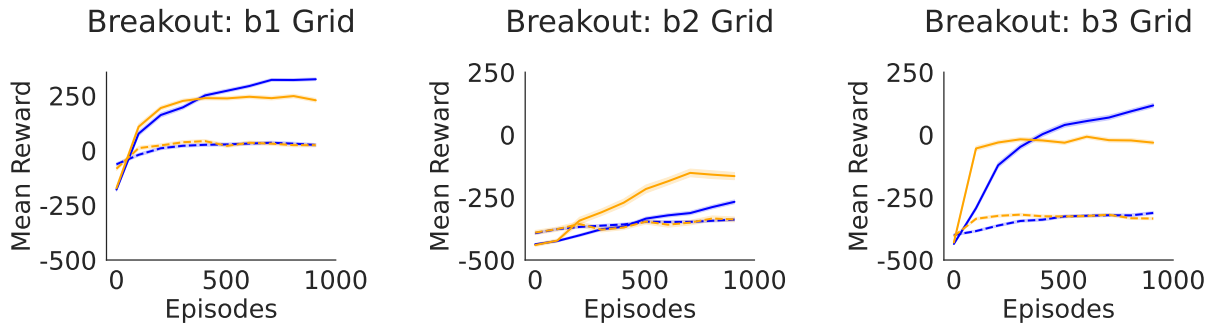


Figure Sup11: *Q-learning Agent with Boltzmann exploration strategy*: Results for Breakout b1, b2, b3 grids reporting mean reward as a function of episode number. The agent is trained on the non-noisy version of the environment and tested on different level of noise ( $\delta \sim \mathcal{N}(0, 0.1)$  in Low-Noise and  $\delta \sim \mathcal{N}(0, 0.5)$  in High-Noise settings).

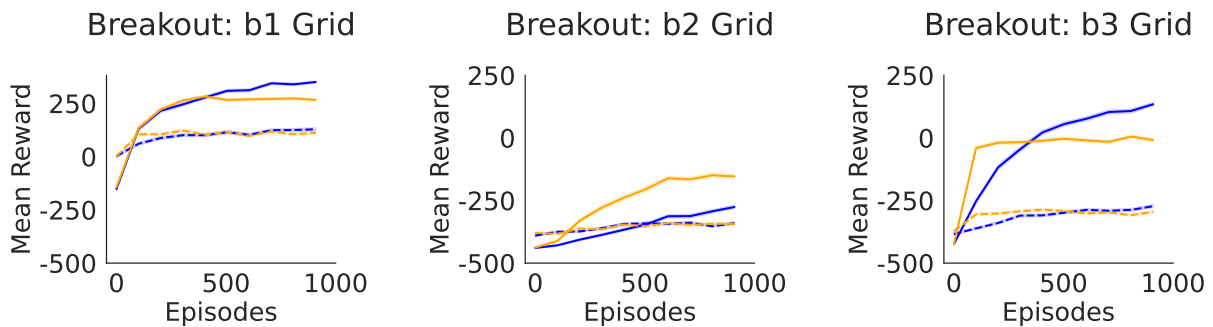


Figure Sup12: *Q-learning Agent with  $\epsilon$ -greedy exploration strategy*: Results for Breakout b1, b2, b3 grids reporting mean reward as a function of episode number. The agent is trained on the non-noisy version of the environment and tested on different level of noise ( $\delta \sim \mathcal{N}(0, 0.1)$  in Low-Noise and  $\delta \sim \mathcal{N}(0, 0.5)$  in High-Noise settings).

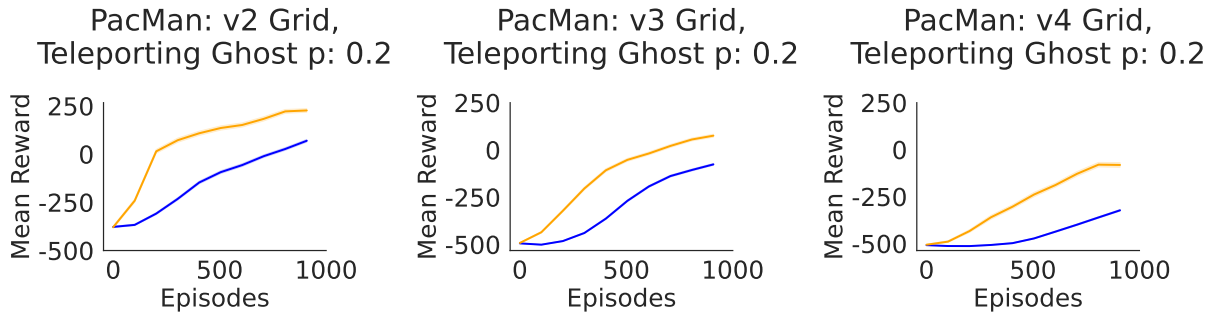


Figure Sup13: *SARSA Agent with Boltzmann exploration strategy*: Results for PacMan v2, v3, v4 grids reporting mean reward as a function of episode number. The agent is trained on the Random Ghost environment and tested on the Teleporting Ghost variation ( $p = 0.2, p = 0.5$ )

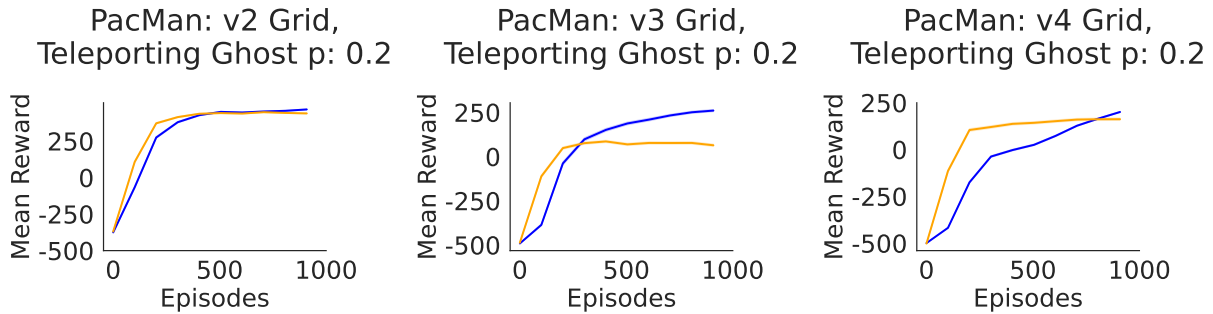


Figure Sup14: *Q-learning Agent with Boltzmann exploration strategy*: Results for PacMan v2, v3, v4 grids reporting mean reward as a function of episode number. The agent is trained on the Random Ghost environment and tested on the Teleporting Ghost variation ( $p = 0.2, p = 0.5$ )

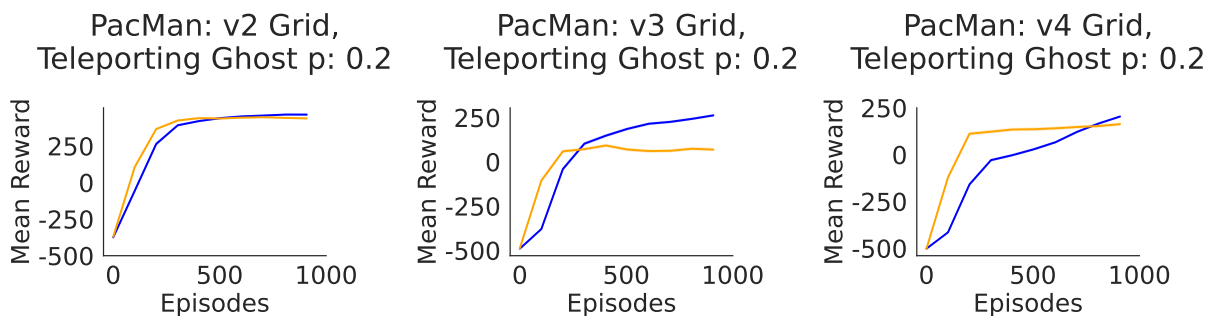


Figure Sup15: *Q-learning Agent with  $\epsilon$ -greedy exploration strategy*: Results for PacMan v2, v3, v4 grids reporting mean reward as a function of episode number. The agent is trained on the Random Ghost environment and tested on the Teleporting Ghost variation ( $p = 0.2, p = 0.5$ )

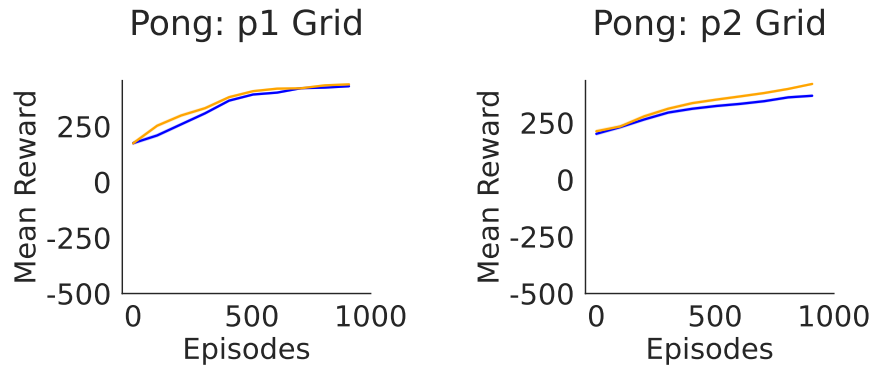


Figure Sup16: *SARSA Agent with Boltzmann exploration strategy*: Results for Pong p1, p2 grids reporting mean reward as a function of episode number. The agent is trained on the Directional Ghost ( $p = 0.3$ ) environment and tested on the Random Ghost variation.

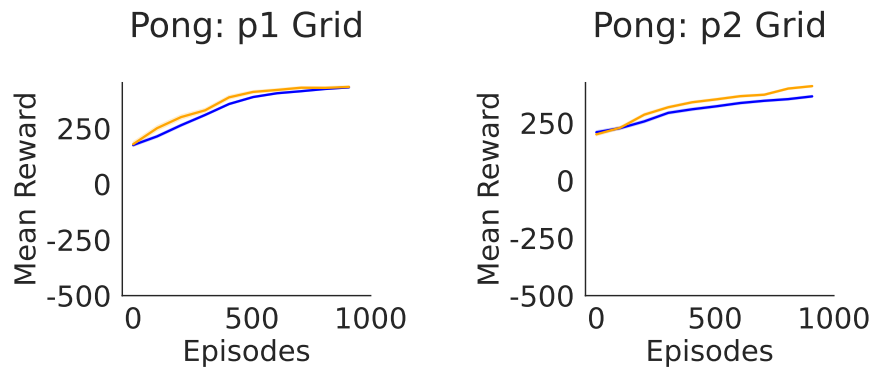


Figure Sup17: *SARSA Agent with  $\epsilon$ -greedy exploration strategy*: Results for Pong p1, p2 grids reporting mean reward as a function of episode number. The agent is trained on the Directional Ghost ( $p = 0.3$ ) environment and tested on the Random Ghost variation.

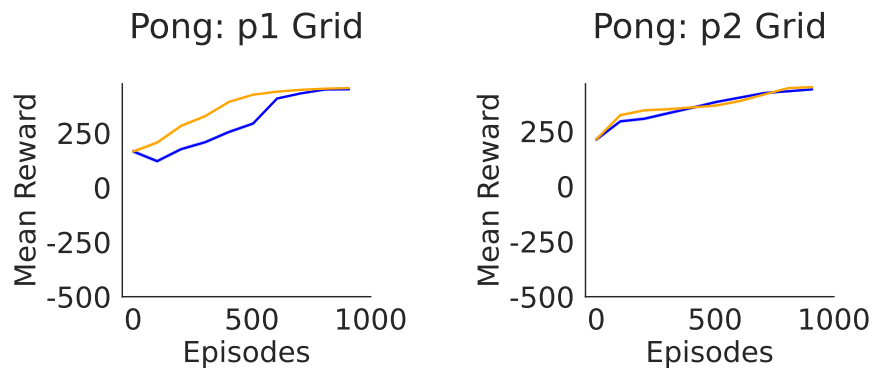


Figure Sup18: *Q-learning Agent with Boltzmann exploration strategy*: Results for Pong p1, p2 grids reporting mean reward as a function of episode number. The agent is trained on the Directional Ghost ( $p = 0.3$ ) environment and tested on the Random Ghost variation.

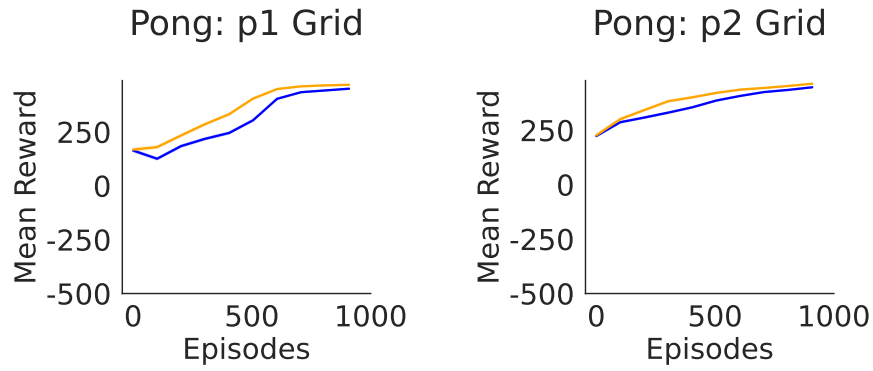


Figure Sup19: *Q-learning Agent with  $\epsilon$ -greedy exploration strategy*: Results for Pong p1, p2 grids reporting mean reward as a function of episode number. The agent is trained on the Directional Ghost ( $p = 0.3$ ) environment and tested on the Random Ghost variation.

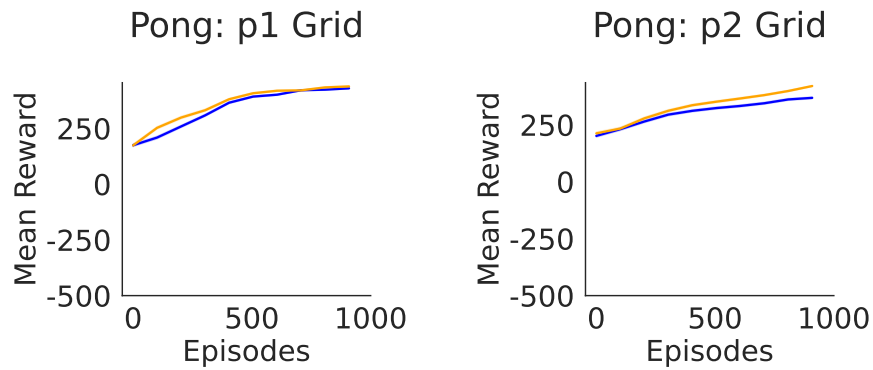


Figure Sup20: *SARSA Agent with  $\epsilon$ -greedy exploration strategy*: Results for Pong p1, p2 grids reporting mean reward as a function of episode number. The agent is trained on the Directional Ghost ( $p = 0.3$ ) environment and tested on the Random Ghost variation.

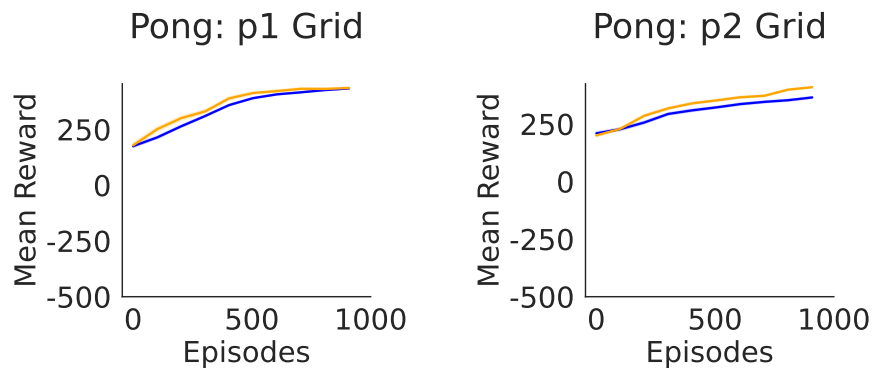


Figure Sup21: *SARSA Agent with  $\epsilon$ -greedy exploration strategy*: Results for Pong p1, p2 grids reporting mean reward as a function of episode number. The agent is trained on the Directional Ghost ( $p = 0.3$ ) environment and tested on the Random Ghost variation.

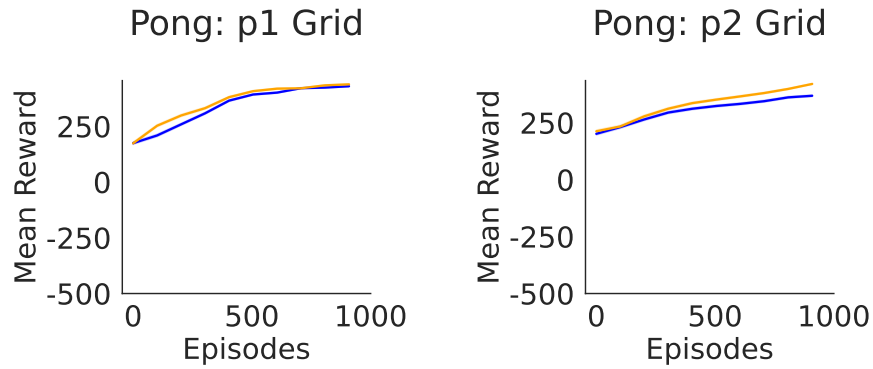


Figure Sup22: *SARSA Agent with  $\epsilon$ -greedy exploration strategy*: Results for Pong p1, p2 grids reporting mean reward as a function of episode number. The agent is trained on the Directional Ghost ( $p = 0.3$ ) environment and tested on the Random Ghost variation.

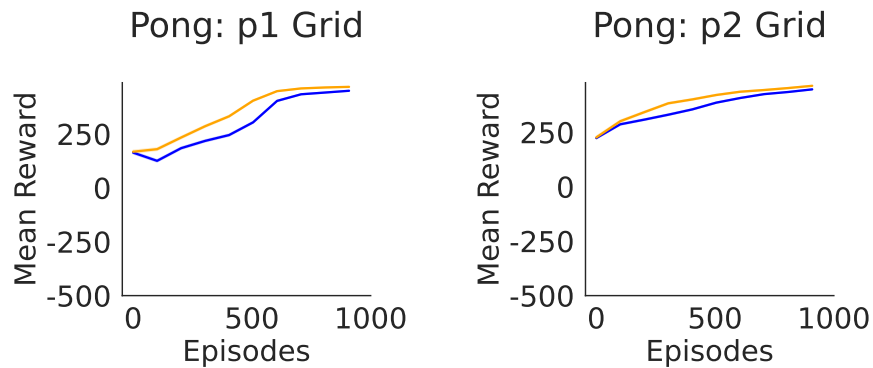


Figure Sup23: *SARSA Agent with  $\epsilon$ -greedy exploration strategy*: Results for Pong p1, p2 grids reporting mean reward as a function of episode number. The agent is trained on the Directional Ghost ( $p = 0.3$ ) environment and tested on the Random Ghost variation.

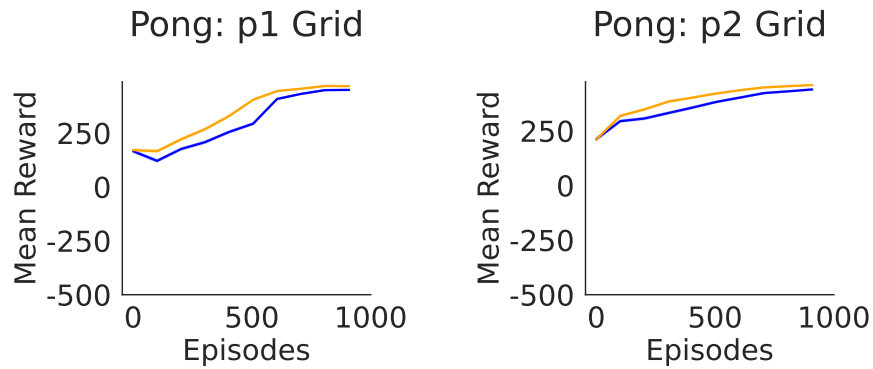


Figure Sup24: *SARSA Agent with  $\epsilon$ -greedy exploration strategy*: Results for Pong p1, p2 grids reporting mean reward as a function of episode number. The agent is trained on the Directional Ghost ( $p = 0.3$ ) environment and tested on the Random Ghost variation.

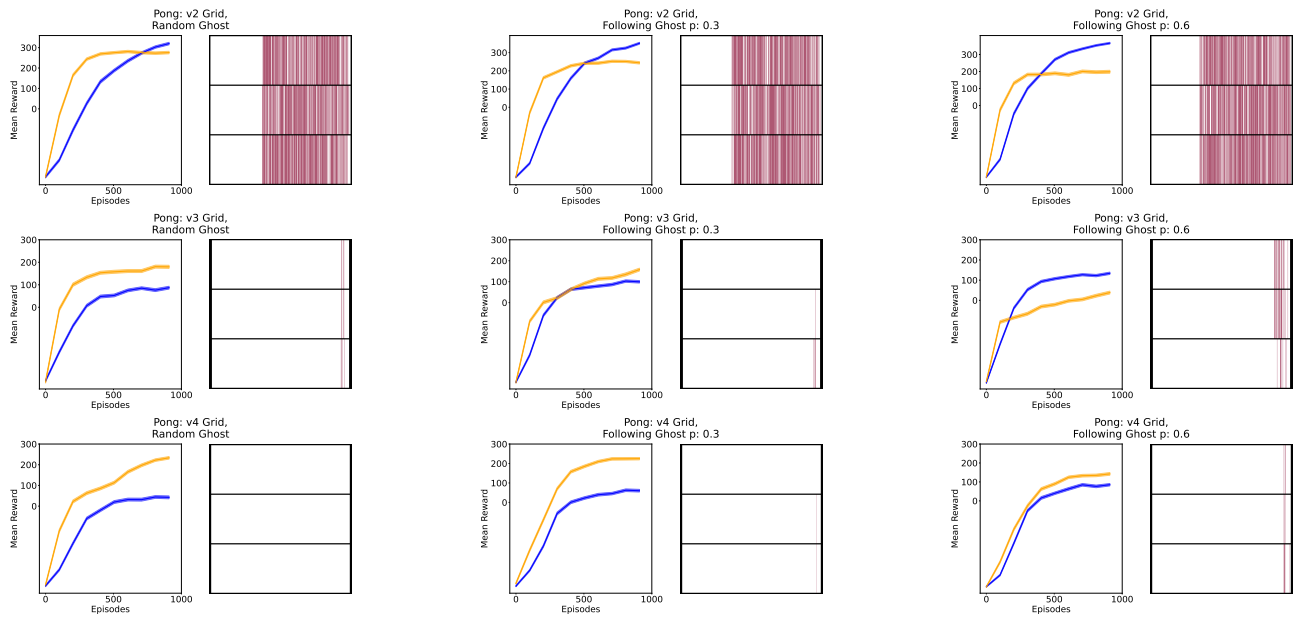


Figure Sup25: *Q-learning Agent with Boltzmann exploration strategy*: The *exploration grid* visualizing the difference in State-Action (S-A) pairs explored by these agents ( $D_{LG}$ ). Results for PacMan v2, v3, v4 grids, the agent is trained on non-noisy variations of different environments (reported in the headings) and tested in the Low-Noise regime. Rows in the right figure represents agent's actions Left, Right, Up, or Down.

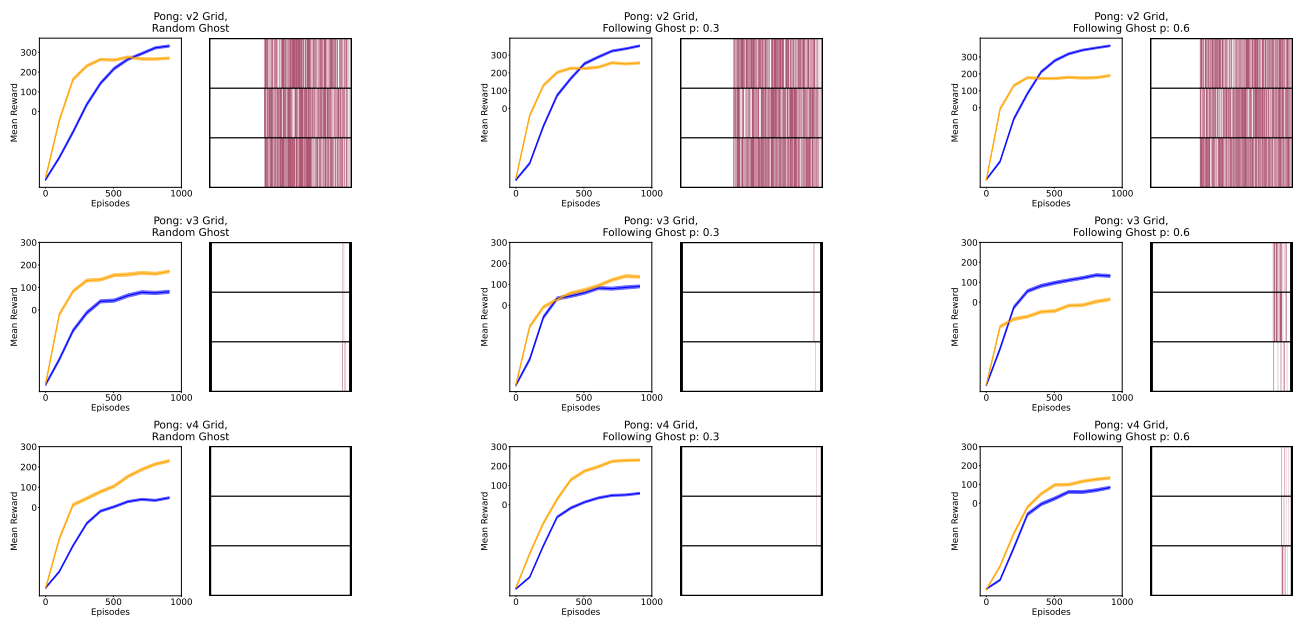


Figure Sup26: *Q-learning Agent with  $\epsilon$ -greedy exploration strategy*: The *exploration grid* visualizing the difference in State-Action (S-A) pairs explored by these agents ( $D_{LG}$ ). Results for PacMan v2, v3, v4 grids, the agent is trained on non-noisy variations of different environments (reported in the headings) and tested in the Low-Noise regime. Rows in the right figure represents agent's actions Left, Right, Up, or Down.

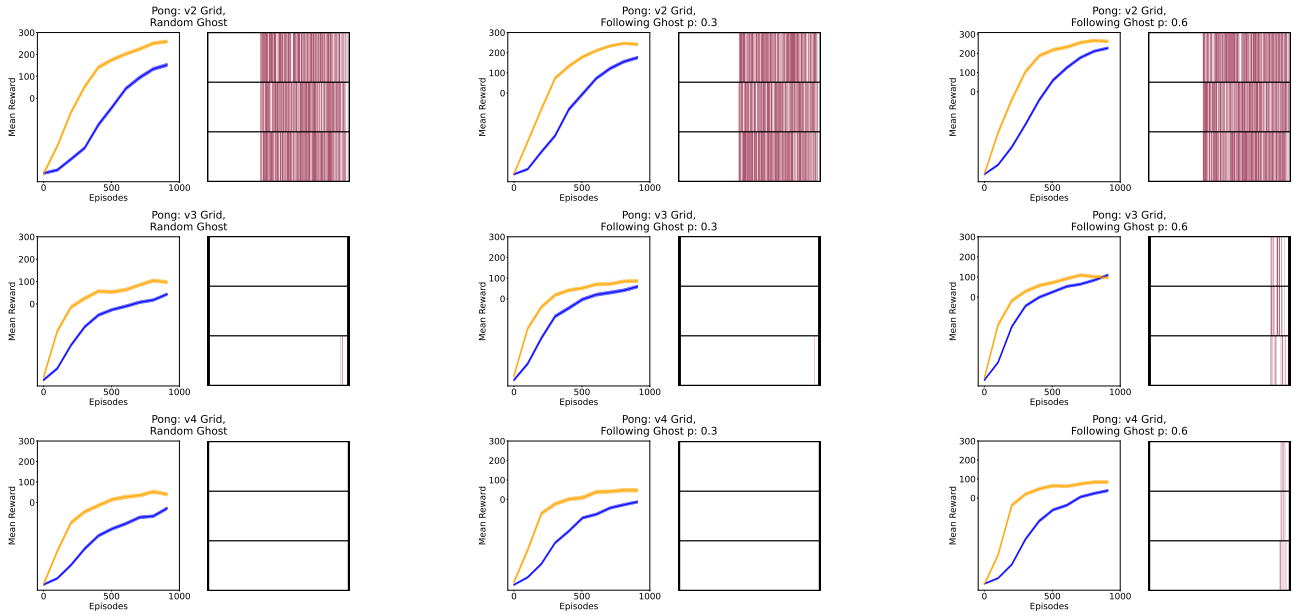


Figure Sup27: SARSA Agent with Boltzmann exploration strategy: The exploration grid visualizing the difference in State-Action (S-A) pairs explored by these agents ( $D_{LG}$ ). Results for PacMan v2, v3, v4 grids, the agent is trained on non-noisy variations of different environments (reported in the headings) and tested in the Low-Noise regime. Rows in the right figure represents agent's actions Left, Right, Up, or Down.

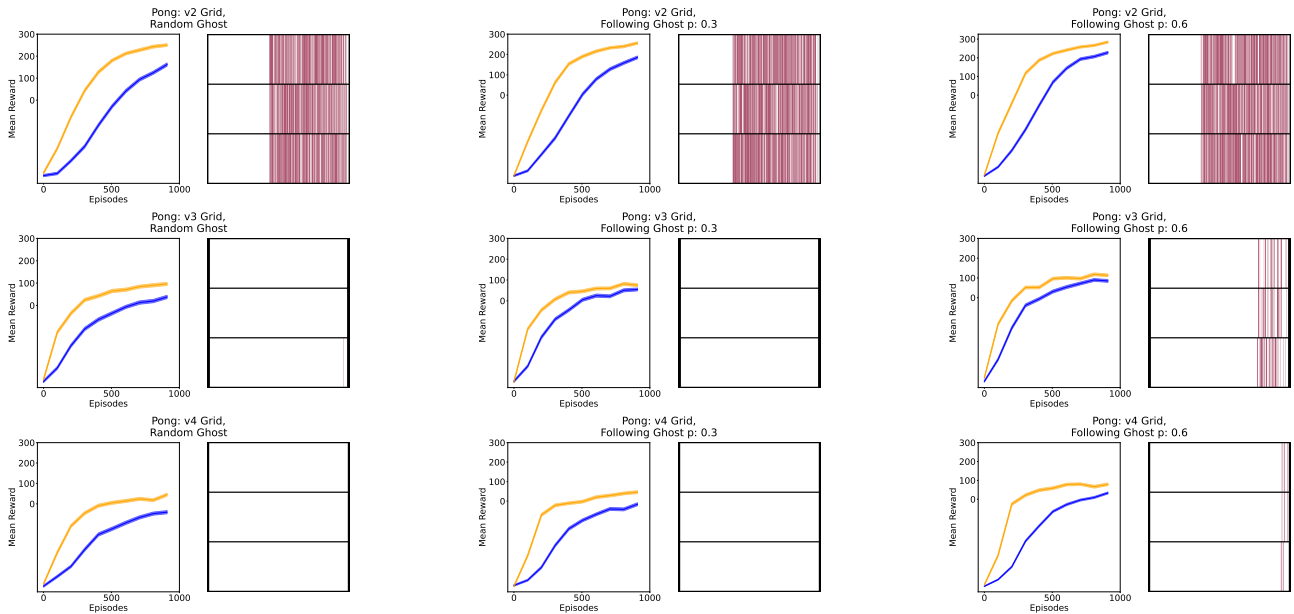


Figure Sup28: SARSA Agent with  $\epsilon$ -greedy exploration strategy: The exploration grid visualizing the difference in State-Action (S-A) pairs explored by these agents ( $D_{LG}$ ). Results for PacMan v2, v3, v4 grids, the agent is trained on non-noisy variations of different environments (reported in the headings) and tested in the Low-Noise regime. Rows in the right figure represents agent's actions Left, Right, Up, or Down.

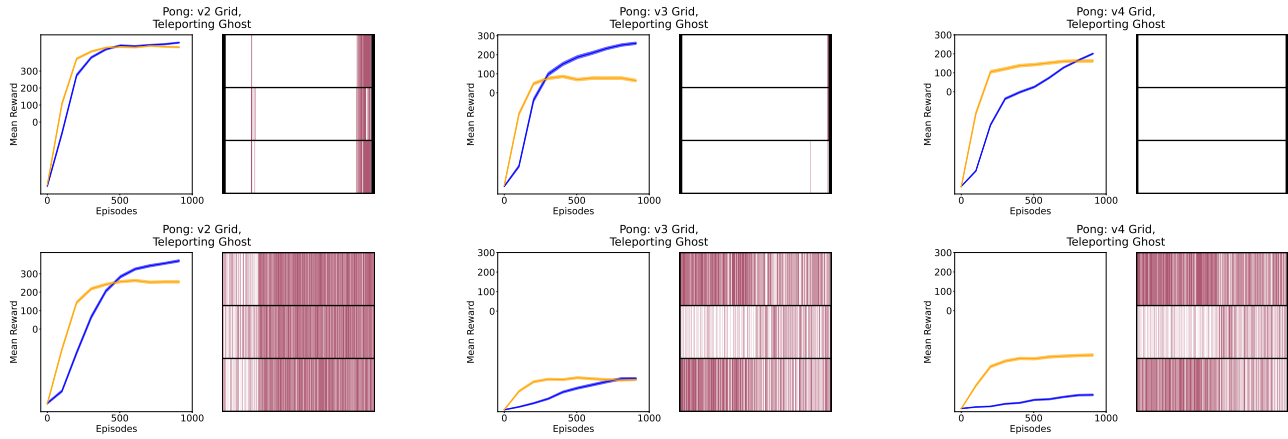


Figure Sup29: *Q-learning Agent with Boltzmann exploration strategy*: The *exploration grid* visualizing the difference in State-Action (S-A) pairs explored by these agents ( $D_{LG}$ ). Results for PacMan v2, v3, v4 grids, the agent is trained on Teleporting Ghost variation ( $p = 0.2, p = 0.5$ ) and tested in different environments (reported in the headings). Rows in the right figure represents agent's actions Left, Right, Up, or Down.

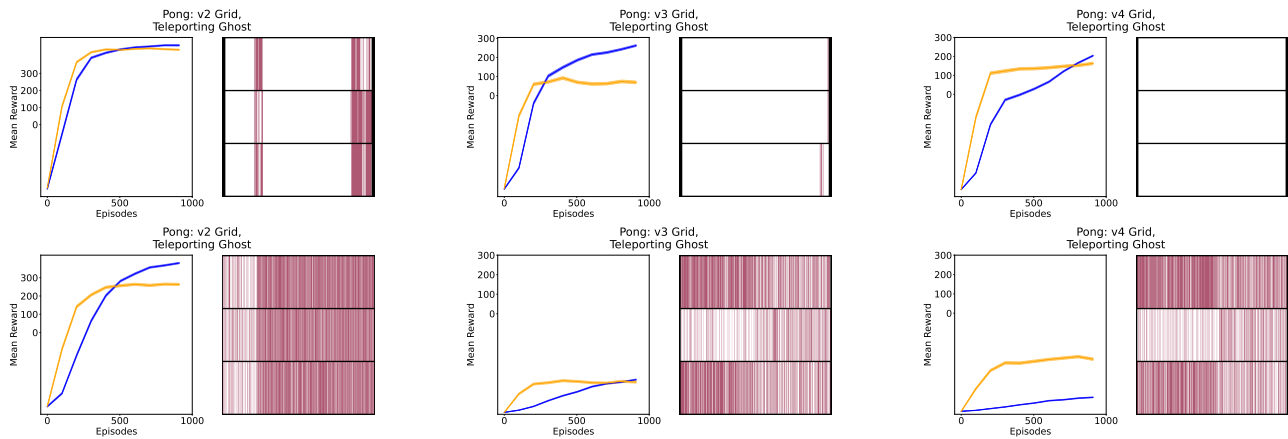


Figure Sup30: *Q-learning Agent with  $\epsilon$ -greedy exploration strategy*: The *exploration grid* visualizing the difference in State-Action (S-A) pairs explored by these agents ( $D_{LG}$ ). Results for PacMan v2, v3, v4 grids, the agent is trained on Teleporting Ghost variation ( $p = 0.2, p = 0.5$ ) and tested in different environments (reported in the headings). Rows in the right figure represents agent's actions Left, Right, Up, or Down.

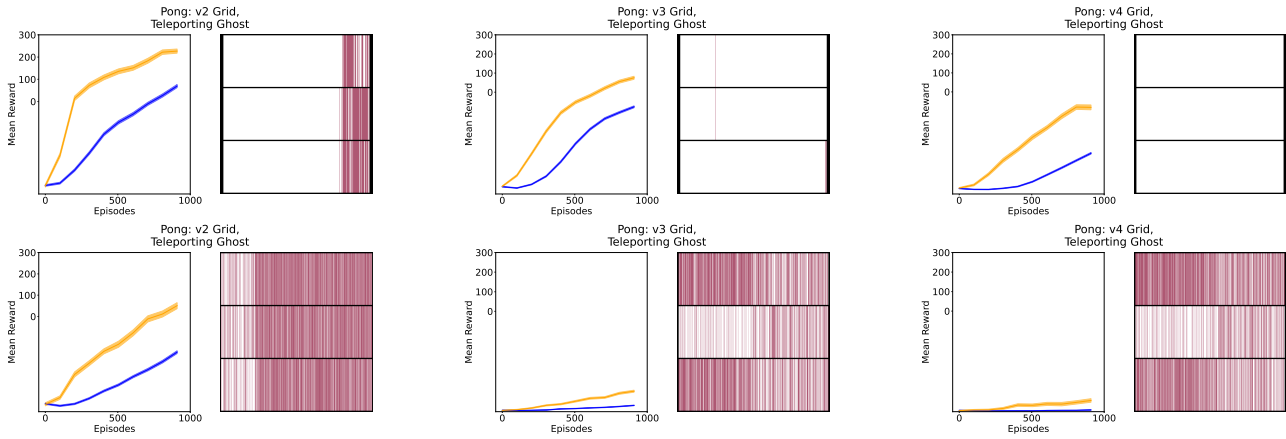


Figure Sup31: *SARSA Agent with Boltzmann exploration strategy*: The *exploration grid* visualizing the difference in State-Action (S-A) pairs explored by these agents ( $D_{LG}$ ). Results for PacMan v2, v3, v4 grids, the agent is trained on Teleporting Ghost variation ( $p = 0.2, p = 0.5$ ) and tested in different environments (reported in the headings). Rows in the right figure represents agent's actions Left, Right, Up, or Down.

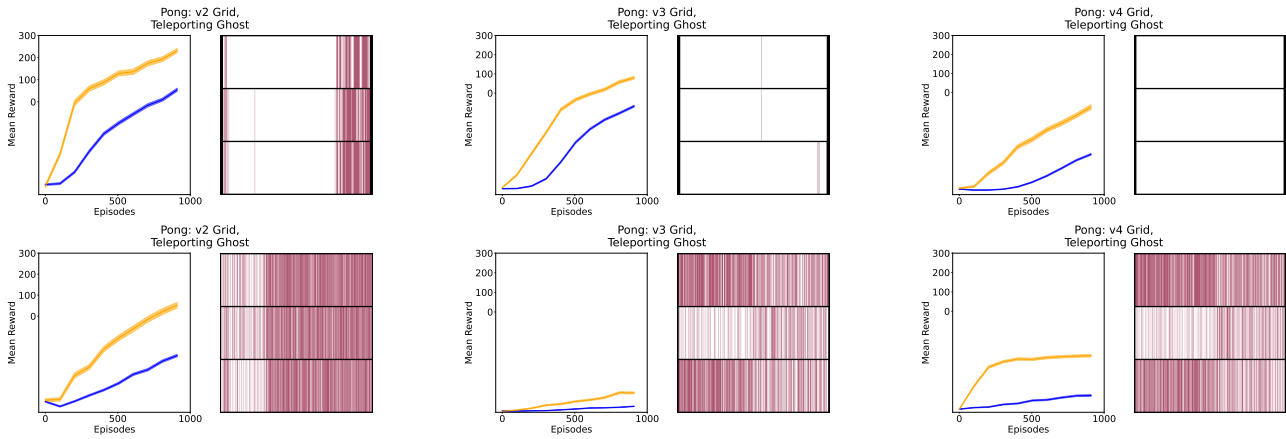


Figure Sup32: *SARSA Agent with  $\epsilon$ -greedy exploration strategy*: The *exploration grid* visualizing the difference in State-Action (S-A) pairs explored by these agents ( $D_{LG}$ ). Results for PacMan v2, v3, v4 grids, the agent is trained on Teleporting Ghost variation ( $p = 0.2, p = 0.5$ ) and tested in different environments (reported in the headings). Rows in the right figure represents agent's actions Left, Right, Up, or Down.

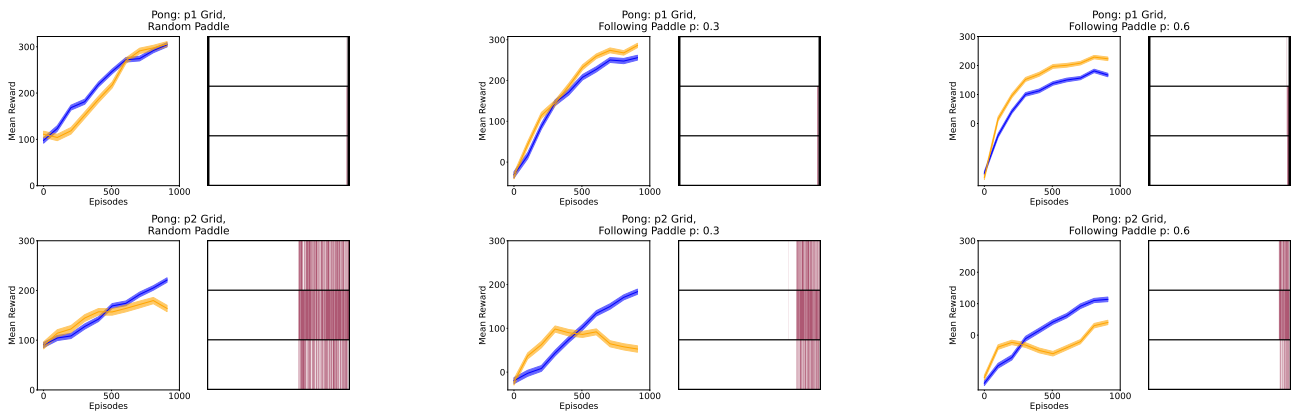


Figure Sup33: *Q-learning Agent with Boltzmann exploration strategy*: The *exploration grid* visualizing the difference in State-Action (S-A) pairs explored by these agents ( $D_{LG}$ ). Results for Pong p1, p2 grids, the agent is trained on non-noisy variations of different environments (reported in the headings) and tested in the Low-Noise regime. Rows in the right figure represents agent's actions Left, Right, Stop.

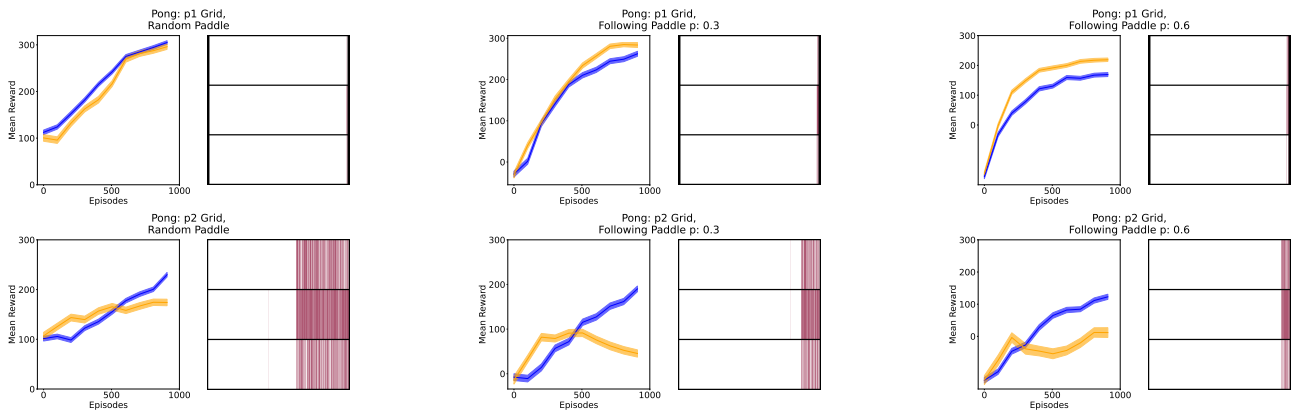


Figure Sup34: *Q-learning Agent with  $\epsilon$ -greedy exploration strategy*: The *exploration grid* visualizing the difference in State-Action (S-A) pairs explored by these agents ( $D_{LG}$ ). Results for Pong p1, p2 grids, the agent is trained on non-noisy variations of different environments (reported in the headings) and tested in the Low-Noise regime. Rows in the right figure represents agent's actions Left, Right, Stop.

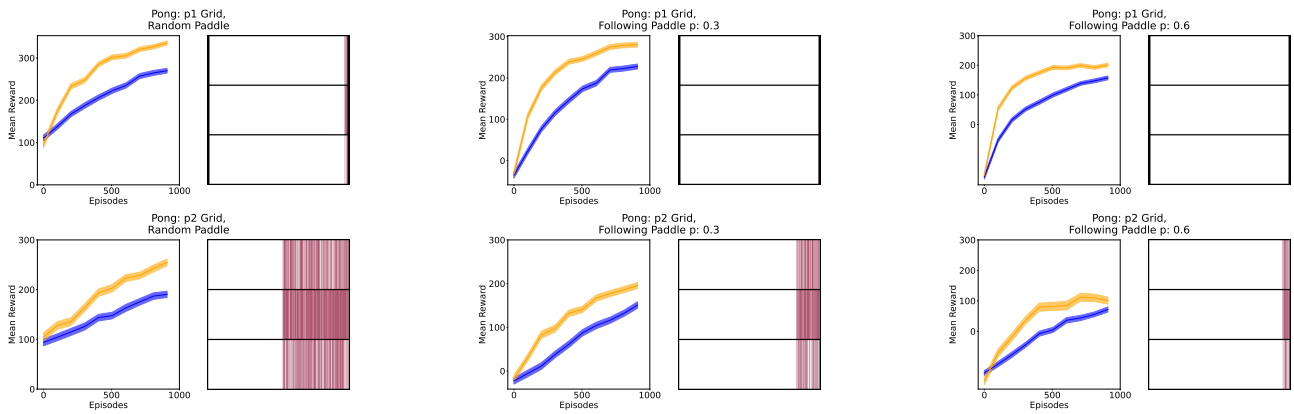


Figure Sup35: *SARSA Agent with Boltzmann exploration strategy*: The *exploration grid* visualizing the difference in State-Action (S-A) pairs explored by these agents ( $D_{LG}$ ). Results for Pong p1, p2 grids, the agent is trained on non-noisy variations of different environments (reported in the headings) and tested in the Low-Noise regime. Rows in the right figure represents agent's actions Left, Right, Stop.

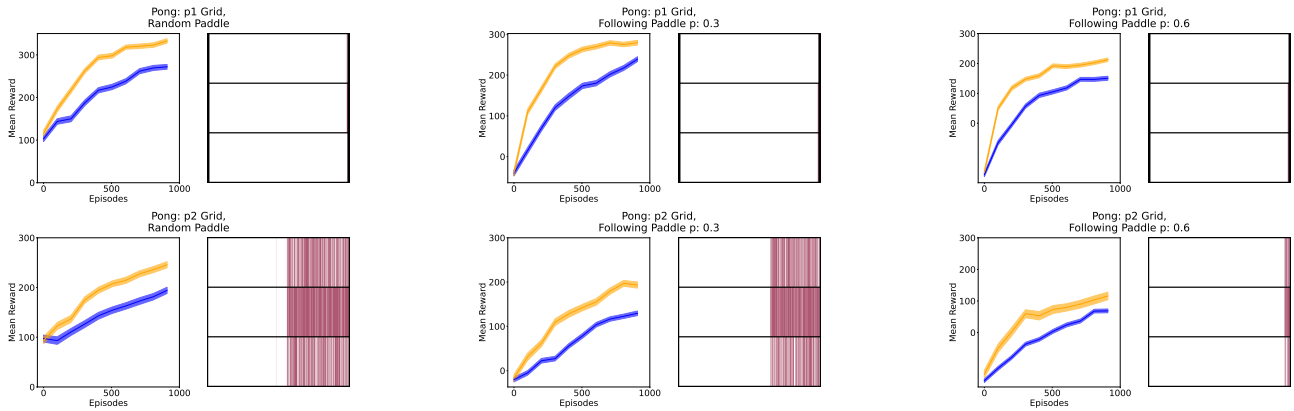


Figure Sup36: *SARSA Agent with  $\epsilon$ -greedy exploration strategy*: The *exploration grid* visualizing the difference in State-Action (S-A) pairs explored by these agents ( $D_{LG}$ ). Results for Pong p1, p2 grids, the agent is trained on non-noisy variations of different environments (reported in the headings) and tested in the Low-Noise regime. Rows in the right figure represents agent's actions Left, Right, Stop.

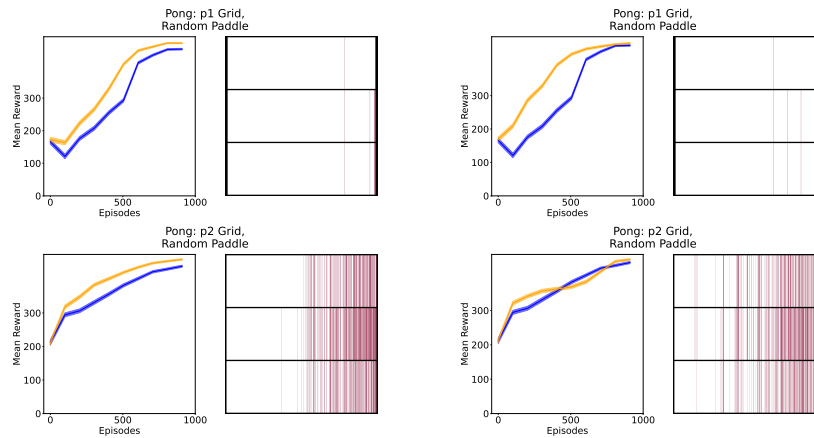


Figure Sup37: *Q-learning Agent with Boltzmann exploration strategy*: The *exploration grid* visualizing the difference in State-Action (S-A) pairs explored by these agents ( $D_{LG}$ ). Results for Pong p1, p2 grids, the agent is trained on Directional paddle ( $p = 0.3$  top,  $p = 0.6$ , bottom) variation and tested in the Random paddle environment. Rows in the right figure represents agent's actions Left, Right, Stop.

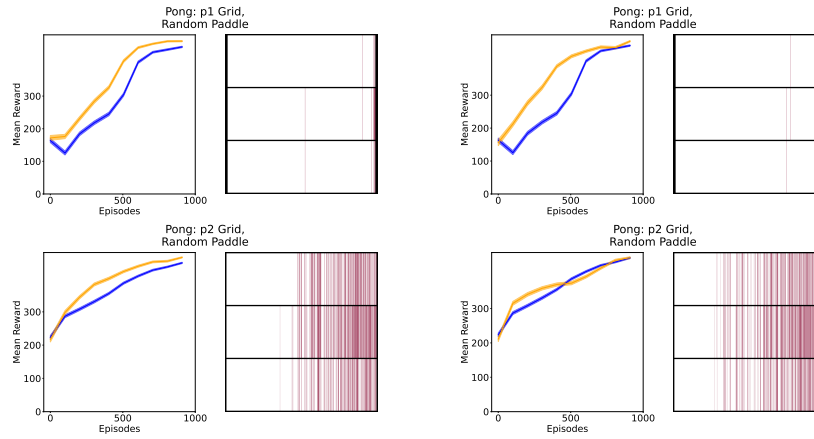


Figure Sup38: *Q-learning Agent with  $\epsilon$ -greedy exploration strategy*: The *exploration grid* visualizing the difference in State-Action (S-A) pairs explored by these agents ( $D_{LG}$ ). Results for Pong p1, p2 grids, the agent is trained on Directional Paddle ( $p = 0.3$  top,  $p = 0.6$ , bottom) variation and tested in the Random Paddle environment. Rows in the right figure represents agent's actions Left, Right, Stop.

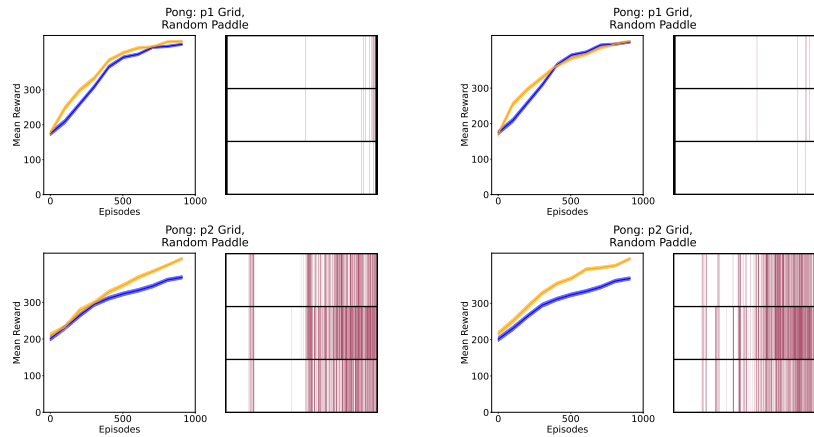


Figure Sup39: *SARSA Agent with Boltzmann exploration strategy*: The *exploration grid* visualizing the difference in State-Action (S-A) pairs explored by these agents ( $D_{LG}$ ). Results for Pong p1, p2 grids, the agent is trained on Directional Paddle ( $p = 0.3$  top,  $p = 0.6$ , bottom) variation and tested in the Random Paddle environment. Rows in the right figure represents agent's actions Left, Right, Stop.

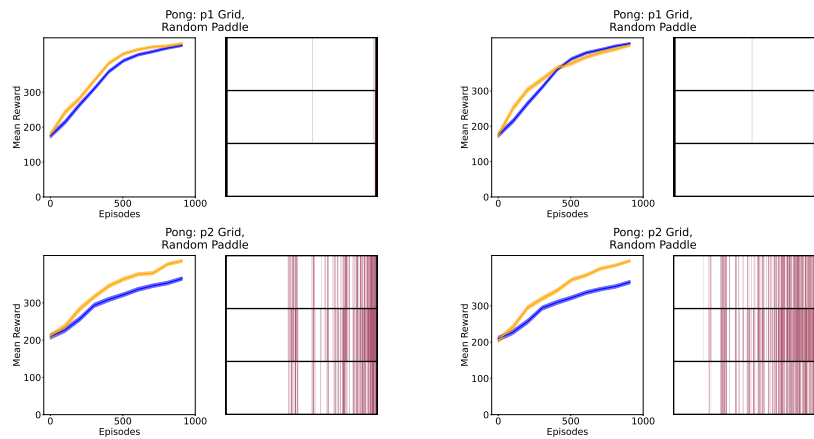


Figure Sup40: *SARSA Agent with  $\epsilon$ -greedy exploration strategy*: The *exploration grid* visualizing the difference in State-Action (S-A) pairs explored by these agents ( $D_{LG}$ ). Results for Pong p1, p2 grids, the agent is trained on Directional Paddle ( $p = 0.3$  top,  $p = 0.6$ , bottom) variation and tested in the Random Paddle environment. Rows in the right figure represents agent's actions Left, Right, Stop.

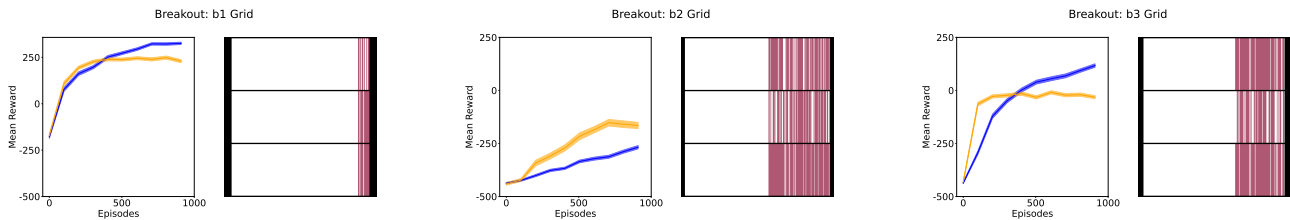


Figure Sup41: *Q-learning Agent with Boltzmann exploration strategy*: The *exploration grid* visualizing the difference in State-Action (S-A) pairs explored by these agents ( $D_{LG}$ ). Results for Breakout b1, b2, b3 grids, the agent is trained on non-noisy variations of different environments (reported in the headings) and tested in the Low-Noise regime. Rows in the right figure represents agent's actions Left, Right, Stop.

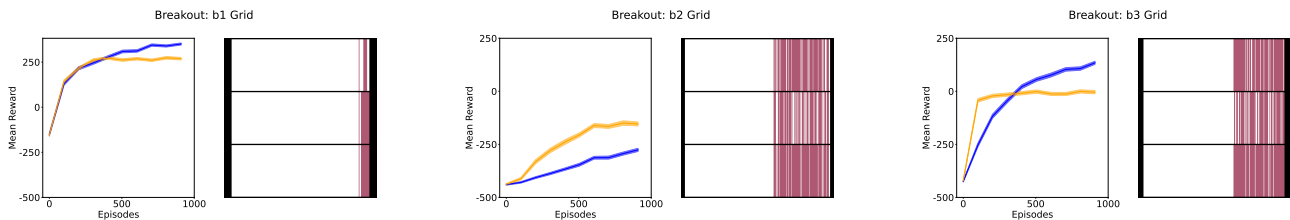


Figure Sup42: *Q-learning Agent with  $\epsilon$ -greedy exploration strategy*: The *exploration grid* visualizing the difference in State-Action (S-A) pairs explored by these agents ( $D_{LG}$ ). Results for Breakout b1, b2, b3 grids, the agent is trained on non-noisy variations of different environments (reported in the headings) and tested in the Low-Noise regime. Rows in the right figure represents agent's actions Left, Right, Stop.

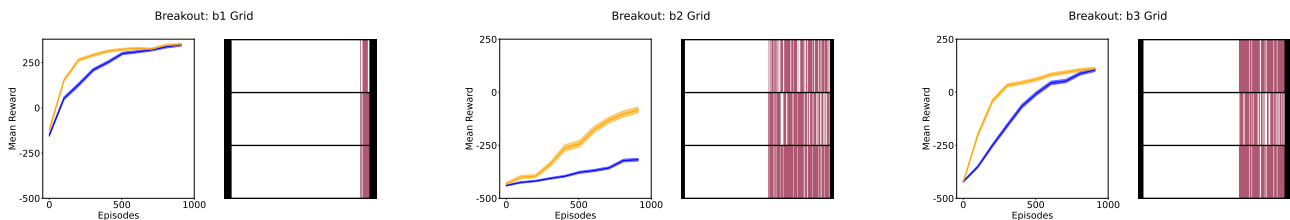


Figure Sup43: *SARSA Agent with Boltzmann exploration strategy*: The *exploration grid* visualizing the difference in State-Action (S-A) pairs explored by these agents ( $D_{LG}$ ). Results for Breakout b1, b2, b3 grids, the agent is trained on non-noisy variations of different environments (reported in the headings) and tested in the Low-Noise regime. Rows in the right figure represents agent's actions Left, Right, Stop.

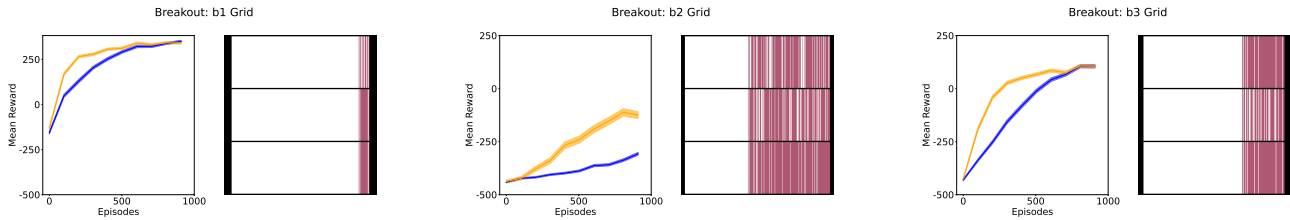


Figure Sup44: *SARSA Agent with  $\epsilon$ -greedy exploration strategy*: The *exploration grid* visualizing the difference in State-Action (S-A) pairs explored by these agents ( $D_{LG}$ ). Results for Breakout b1, b2, b3 grids, the agent is trained on non-noisy variations of different environments (reported in the headings) and tested in the Low-Noise regime. Rows in the right figure represents agent's actions Left, Right, Stop.

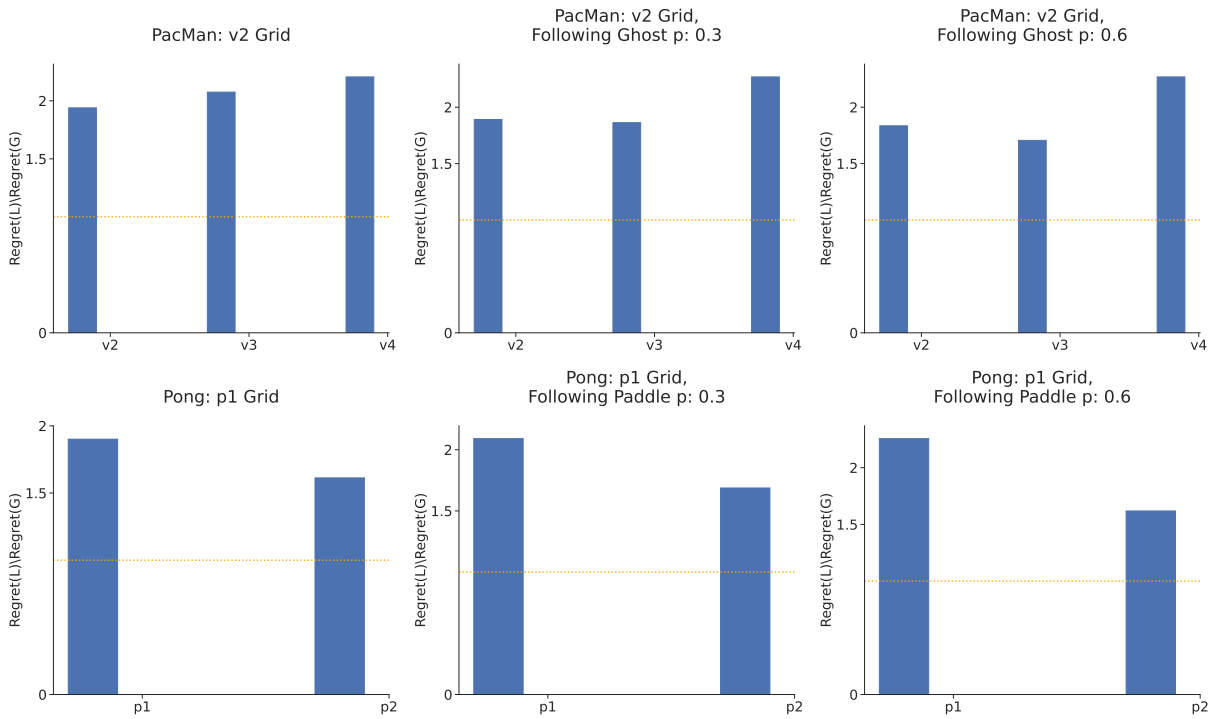


Figure Sup45: *Regret for SARSA Agent with  $\epsilon$ -greedy exploration strategy across non-semantic game variations*: Results for Pac-Man (v2, v3, v4) and Pong (p1, p2) grids, showing the ratio of regrets between Learnability and Generalization agents (L/G). The agents were trained in the Random Ghost/ Random Bar environment without perturbation and tested in the Low-Noise regime.

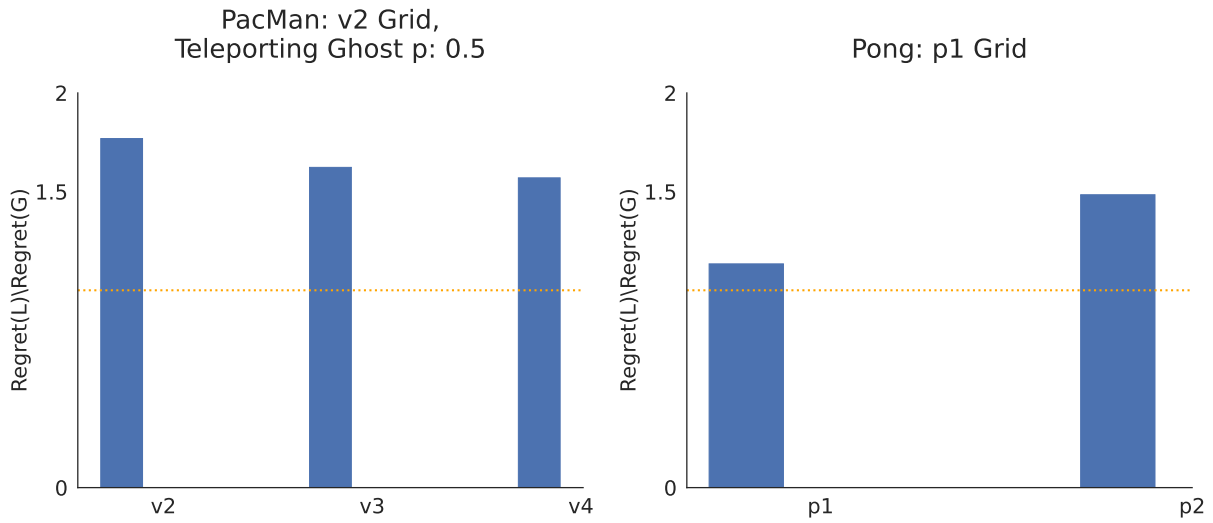


Figure Sup46: *Regret for SARSA Agent with  $\epsilon$ -greedy exploration strategy across semantic game variations*: Results for Pac-Man (v2, v3, v4) and Pong (p1, p2) grids, showing the ratio of regrets between Learnability and Generalization agents (L/G). The agents were trained in the Random Ghost/ Random Bar environment and tested in the Teleporting Ghost/Directional Paddle ( $p = 0.3$  top,  $p = 0.6$ , bottom) environments.

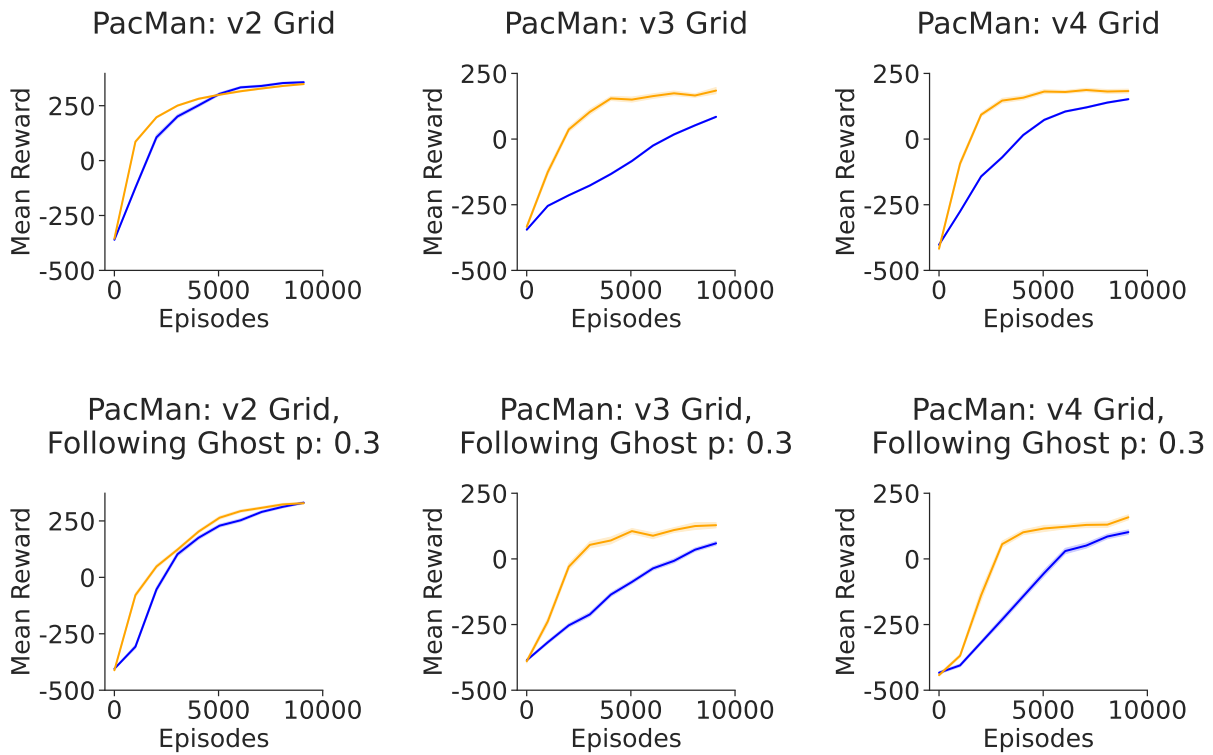


Figure Sup47: *DQN Agent with  $\epsilon$ -greedy exploration strategy across non-semantic variations*: Results for PacMan v2, v3, v4 grids reporting mean reward as a function of episode number. The agent is trained on the non-noisy version of the environment and tested on different level of noise ( $\delta \sim \mathcal{N}(0, 0.1)$  in Low-Noise and  $\delta \sim \mathcal{N}(0, 0.5)$  in High-Noise settings)

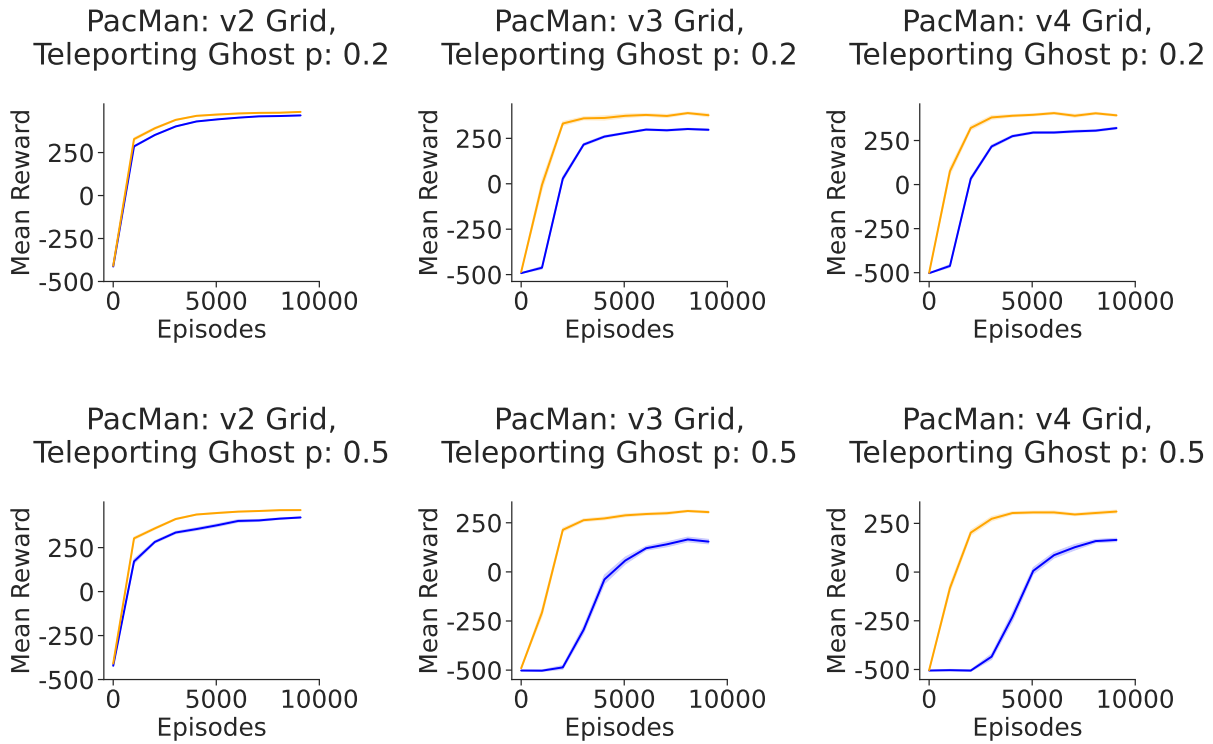


Figure Sup48: *DQN Agent with  $\epsilon$ -greedy exploration strategy across semantic variations*: Results for PacMan v2, v3, v4 grids reporting mean reward as a function of episode number. The agent is trained on the Random Ghost environment and tested on the Teleporting Ghost variation ( $p = 0.2, p = 0.5$ )

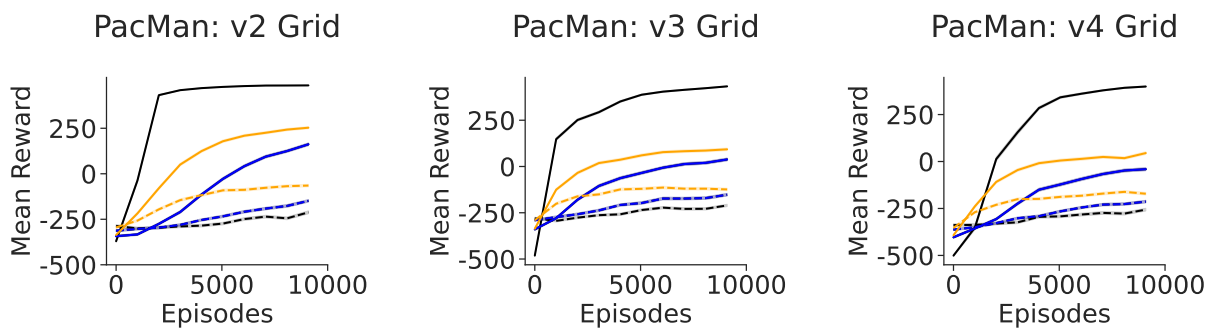


Figure Sup49: *SARSA Agent with  $\epsilon$ -greedy exploration strategy*: Results for Pac-Man (v2, v3, v4) grids showing the mean reward as a function of episode number. The agent is trained in the non-noisy environment and tested under varying noise levels: Low-Noise ( $\delta \sim \mathcal{N}(0, 0.1)$ ), High-Noise ( $\delta \sim \mathcal{N}(0, 0.5)$ ), and the extremes of maximum noise ( $\delta \sim \mathcal{N}(0, 1)$ ) and no noise ( $\delta \sim \mathcal{N}(0, 0)$ ), represented in black.

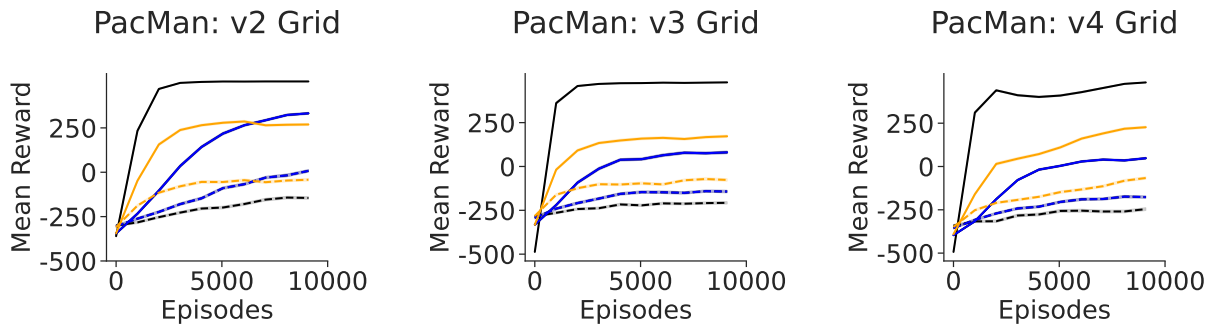


Figure Sup50: *Boltzmann Agent with  $\epsilon$ -greedy exploration strategy*: Results for Pac-Man (v2, v3, v4) grids showing the mean reward as a function of episode number. The agent is trained in the non-noisy environment and tested under varying noise levels: Low-Noise ( $\delta \sim \mathcal{N}(0, 0.1)$ ), High-Noise ( $\delta \sim \mathcal{N}(0, 0.5)$ ), and the extremes of maximum noise ( $\delta \sim \mathcal{N}(0, 1)$ ) and no noise ( $\delta \sim \mathcal{N}(0, 0)$ ), represented in black.

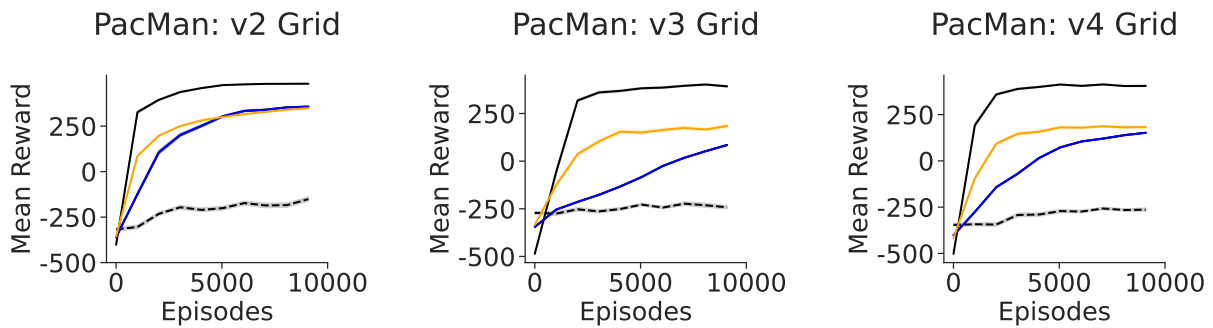


Figure Sup51: *DQN Agent with  $\epsilon$ -greedy exploration strategy*: Results for Pac-Man (v2, v3, v4) grids showing the mean reward as a function of episode number. The agent is trained in the non-noisy environment and tested under varying noise levels: Low-Noise ( $\delta \sim \mathcal{N}(0, 0.1)$ ), High-Noise ( $\delta \sim \mathcal{N}(0, 0.5)$ ), and the extremes of maximum noise ( $\delta \sim \mathcal{N}(0, 1)$ ) and no noise ( $\delta \sim \mathcal{N}(0, 0)$ ), represented in black.